NASA Technical Paper 1758

# Pseudosteady-State Analysis of Nonlinear Aircraft Maneuvers

John W. Young, Albert A. Schy,
and Katherine G. Johnson

DECEMBER 1980

NASA

NASA Technical Paper 1758

# Pseudosteady-State Analysis of Nonlinear Aircraft Maneuvers

John W. Young, Albert A. Schy,
and Katherine G. Johnson
*Langley Research Center*
*Hampton, Virginia*

## SUMMARY

An analytical method has been developed for studying the combined effects of rotational coupling and nonlinear aerodynamics on aircraft response for specified control inputs. The method involves the simultaneous solution of two nonlinear equations which are functions of angle of attack, roll rate, and control inputs. The method is applied to a number of maneuvers for a fighter-type aircraft. Time history responses verified the usefulness of the analysis for predicting a variety of response characteristics caused by interacting nonlinear aerodynamic and inertial effects, including spin conditions.

## INTRODUCTION

Maneuvering aircraft sometimes undergo sudden divergent motions not predicted by linearized response analysis. The basic theory explaining this nonlinear response was established by Phillips in reference 1. The analysis of reference 1 predicted that divergentlike motions would occur for certain critical roll rates when the linearized analysis predicted satisfactory behavior. Numerous extensions have been made to Phillips' analysis (for example, refs. 2 to 5). These studies showed that Phillips' critical roll rates were related to pseudosteady solutions of the equations of motion and that the divergences ("jump" phenomena) observed in simulated maneuver calculations were transitions from one pseudosteady solution to another. These studies considered roll rate as the basic independent variable, and their main objective was to predict peak values of the incidence angles, $\beta$ and $\alpha$, in the vicinity of the critical values of roll rate. However, the pseudosteady values were found to be poor estimates of these critical peak values. The reason for this disagreement was shown in reference 6. An elegant perturbation expansion of the weight-component variations was used to show that these variations were very important in estimating peak values of $\alpha$ and $\beta$ for constant roll rates near the critical values. The fact that weight-component variations are ignored in pseudosteady-state analysis explained the failure of the previous studies. However, the method of reference 6 is also of limited usefulness in predicting peak values in critical rotational maneuvers because it is based on the assumption of constant roll rate. Many simulator studies have shown that for critical combinations of control inputs, all the coupled responses, including roll rate, are very irregular, so that calculations based on constant roll rate are not realistic.

In reference 7, Schy and Hannah took a different approach to the application of pseudosteady-state (PSS) analysis. They found that the quantitative calculations of peak values can best be performed by computer integration of the nonlinear differential equations, but the pseudosteady-state analysis could

be very useful in the qualitative analysis of critical rotationally coupled maneuvers and in obtaining approximate values for critical control combinations. Multiple pseudosteady solutions were plotted over the domain of allowable control inputs, and critical control combinations were identified as those for which there was a tendency to diverge from the normal response regime toward another solution regime corresponding to some highly coupled, nonlinear response. Stability characteristics of each solution were also shown to be useful in interpreting the pseudosteady results. Although it was shown in reference 7 that the method could be extended to include nonlinear aerodynamic effects, the results presented were based on the assumption of linear aerodynamics.

The analysis of reference 7 was extended in reference 8 to include aerodynamics which were nonlinear in angle of attack. Although it was assumed in reference 8 that the PSS solutions were mainly useful in considering rapid rotational maneuvers as nonlinear perturbations from horizontal flight, it was shown that the PSS analysis also yielded high-angle-of-attack, spinlike solutions. However, the equations of motion and aerodynamics used in reference 8 were inadequate to represent the high-angle-of-attack regime.

In references 9 and 10, Mehra and his co-workers have shown that catastrophe and bifurcation theory can be applied to pseudosteady-state analysis of airplane maneuvers. They have developed a sophisticated computer program, based on continuation theory, for calculating both pseudosteady and truly steady solutions and have shown results for several example cases. The method of references 9 and 10 allows for nonlinear aerodynamics and is highly mathematical in nature.

In the present study, the emphasis is on the physical and engineering interpretation of the theory and results, with a minimum of mathematical sophistication. The objective is to extend the preliminary analysis of reference 8 by giving a more detailed presentation and description of the results. The method of reference 8 is rederived using a more realistic dynamic and aerodynamic representation. The present study confirms that the spinlike PSS solutions at high angles of attack do approximate the true equilibrium spin conditions for the aircraft when the aerodynamics are represented realistically. Therefore, to the extent that variation with angle of attack adequately represents the nonlinear aerodynamics, the PSS method provides an effective means for surveying maneuver characteristics and their stability properties (for any combination of control inputs) over the whole regime of angle of attack. If more variables are needed to define the nonlinear aerodynamics, then the PSS solution would have to be extended to include these as independent variables.

PSS solutions are given for a variety of pitch and roll maneuvers of a fighter-type aircraft, and time history responses are presented to validate the PSS prediction procedure.

2

## SYMBOLS

All aerodynamic data and flight motions are referenced to the principal axis system.

$[A]$ — characteristic stability matrix, equation (12)

$\left.\begin{array}{l} A_0, A_1, A_2 \\ A_3, A_4, A_5 \end{array}\right\}$ — coefficients of polynomial equation (11)

$\left.\begin{array}{l} B_0, B_1 \\ B_2, B_3 \end{array}\right\}$ — coefficients in equation (10) defining $\bar{\beta}$

$b$ — wing span

$C_l$ — rolling-moment coefficient

$C_m$ — pitching-moment coefficient

$C_n$ — yawing-moment coefficient

$C_{n\beta,dyn}$ — $= C_{n\beta} - \dfrac{I_Z}{I_X} C_{l\beta} \sin \alpha$

$C_X$ — longitudinal-force coefficient

$C_Y$ — side-force coefficient

$C_Z$ — vertical-force coefficient

$\bar{c}$ — mean aerodynamic chord

$D$ — drag

$D_0, D_2$ — coefficients of equation (7)

$E_a$ — aileron effectiveness parameter, $C_{n\beta} - C_{l\beta} C_{n\delta_a} / C_{l\delta_a}$

$g$ — acceleration due to gravity

$I_X, I_Y, I_Z, I_{XZ}$ — body-axis moments and product of inertia about center of mass

$J_X$ — $= (I_Z - I_Y)/I_X$

$J_Y$ — $= (I_Z - I_X)/I_Y$

$J_Z$ $= (I_Y - I_X)/I_Z$

m          mass of aircraft

p,q,r      body-axis rolling, pitching, and yawing angular rates

$Q_0, Q_1, Q_2$   coefficients in equation (8) defining $\bar{q}$

$q_\infty$   dynamic pressure, $\frac{1}{2}\rho V^2$

$R_0, R_1$   coefficients in equation (9) defining $\bar{r}$

S          wing area

t          time

V          airspeed

W          weight of aircraft

$\alpha$          angle of attack

$\beta$          angle of sideslip

$\Delta$          determinant of matrix, equation (7)

$\gamma$          flight-path angle

$\delta_a$          aileron deflection, positive when right aileron trailing edge is down

$\delta_e$          elevator deflection, positive when trailing edge is down

$\Delta\delta_e$          elevator increment from one-g trim condition ($\Delta\delta_e = \delta_e + 3.1°$)

$\delta_r$          rudder deflection, positive when trailing edge is left

$\rho$          air density

$\phi, \theta$      Euler angles

$\omega$          angular velocity, $(p^2 + q^2 + r^2)^{1/2}$

Coefficients and derivatives:

$$C_{l_{\delta_a}} = \frac{\partial C_l}{\partial \delta_a} \qquad l_{\delta_a} = \frac{q_\infty S b}{I_X} C_{l_{\delta_a}} \qquad \hat{l}_{\delta_a} = \frac{l_{\delta_a}}{J_X}$$

$$c_{l_{\delta_r}} = \frac{\partial c_l}{\partial \delta_r} \qquad l_{\delta_r} = \frac{q_\infty S b}{I_X} c_{l_{\delta_r}} \qquad \hat{l}_{\delta_r} = \frac{l_{\delta_r}}{J_X}$$

$$c_{l_\beta} = \frac{\partial c_l}{\partial \beta} \qquad l_\beta = \frac{q_\infty S b}{I_X} c_{l_\beta} \qquad \hat{l}_\beta = \frac{l_\beta}{J_X}$$

$$c_{l_p} = \frac{\partial c_l}{\partial \frac{pb}{2V}} \qquad l_p = \frac{q_\infty S b}{I_X} \frac{b}{2V} c_{l_p} \qquad \hat{l}_p = \frac{l_p}{J_X}$$

$$c_{l_r} = \frac{\partial c_l}{\partial \frac{rb}{2V}} \qquad l_r = \frac{q_\infty S b}{I_X} \frac{b}{2V} c_{l_r} \qquad \hat{l}_r = \frac{l_r}{J_X}$$

$$\hat{l}_0 = \hat{l}_{\delta_a} \delta_a + \hat{l}_{\delta_r} \delta_r$$

$$m = \frac{q_\infty S \bar{c}}{I_Y} c_m \qquad \hat{m} = \frac{m}{J_Y}$$

$$c_{m_{\delta_e}} = \frac{\partial c_m}{\partial \delta_e} \qquad m_{\delta_e} = \frac{q_\infty S \bar{c}}{I_Y} c_{m_{\delta_e}} \qquad \hat{m}_{\delta_e} = \frac{m_{\delta_e}}{J_Y}$$

$$c_{m_q} = \frac{\partial c_m}{\partial \frac{q\bar{c}}{2V}} \qquad m_q = \frac{q_\infty S \bar{c}}{I_Y} \frac{\bar{c}}{2V} c_{m_q} \qquad \hat{m}_q = \frac{m_q}{J_Y}$$

$$\hat{m}_0 = \hat{m} + \hat{m}_{\delta_e} \delta_e$$

$$c_{n_{\delta_a}} = \frac{\partial c_n}{\partial \delta_a} \qquad n_{\delta_a} = \frac{q_\infty S b}{I_Z} c_{n_{\delta_a}} \qquad \hat{n}_{\delta_a} = \frac{n_{\delta_a}}{J_Z}$$

5

$$c_{n_{\delta_r}} = \frac{\partial c_n}{\partial \delta_r} \qquad n_{\delta_r} = \frac{q_\infty Sb}{I_z} c_{n_{\delta_r}} \qquad \hat{n}_{\delta_r} = \frac{n_{\delta_r}}{J_z}$$

$$c_{n_\beta} = \frac{\partial c_n}{\partial \beta} \qquad n_\beta = \frac{q_\infty Sb}{I_z} c_{n_\beta} \qquad \hat{n}_\beta = \frac{n_\beta}{J_z}$$

$$c_{n_p} = \frac{\partial c_n}{\partial \frac{pb}{2V}} \qquad n_p = \frac{q_\infty Sb}{I_z} \frac{b}{2V} c_{n_p} \qquad \hat{n}_p = \frac{n_p}{J_z}$$

$$c_{n_r} = \frac{\partial c_n}{\partial \frac{rb}{2V}} \qquad n_r = \frac{q_\infty Sb}{I_z} \frac{b}{2V} c_{n_r} \qquad \hat{n}_r = \frac{n_r}{J_z}$$

$$\hat{n}_0 = \hat{n}_{\delta_a} \delta_a + \hat{n}_{\delta_r} \delta_r$$

$$X = \frac{q_\infty S}{mV} c_X$$

$$c_{X_{\delta_e}} = \frac{\partial c_X}{\partial \delta_e} \qquad X_{\delta_e} = \frac{q_\infty S}{mV} c_{X_{\delta_e}}$$

$$Z = \frac{q_\infty S}{mV} c_Z$$

$$c_{Z_{\delta_e}} = \frac{\partial c_Z}{\partial \delta_e} \qquad Z_{\delta_e} = \frac{\bar{q} S}{mV} c_{Z_{\delta_e}}$$

$$z_0 = \left[ Z + Z_{\delta_e} \delta_e \right] \cos \alpha - \left[ X + X_{\delta_e} \delta_e \right] \sin \alpha$$

$$c_{Y_{\delta_a}} = \frac{\partial c_Y}{\partial \delta_a} \qquad Y_{\delta_a} = \frac{q_\infty S}{mV} c_{Y_{\delta_a}}$$

$$C_{Y_{\delta_r}} = \frac{\partial C_Y}{\partial \delta_r} \qquad\qquad Y_{\delta_r} = \frac{q_\infty S}{mV} C_{Y_{\delta_r}}$$

$$C_{Y_\beta} = \frac{\partial C_Y}{\partial \beta} \qquad\qquad Y_\beta = \frac{q_\infty S}{mV} C_{Y_\beta}$$

$$C_{Y_p} = \frac{\partial C_Y}{\partial \dfrac{pb}{2V}} \qquad\qquad Y_p = \frac{q_\infty S}{mV} \frac{b}{2V} C_{Y_p}$$

$$C_{Y_r} = \frac{\partial C_Y}{\partial \dfrac{rb}{2V}} \qquad\qquad Y_r = \frac{q_\infty S}{mV} \frac{b}{2V} C_{Y_r}$$

$$Y_0 = Y_{\delta_a}\delta_a + Y_{\delta_r}\delta_r$$

Subscript:

$\alpha$        partial derivative with respect to angle of attack

A dot over a symbol indicates a derivative with respect to time.  A bar over a symbol indicates a pseudosteady-state solution.

## PROBLEM FORMULATION AND SOLUTION

An analytical method for finding approximate steady-state solutions to the nonlinear equations of motion of an aircraft in maneuvering flight is discussed in this section.  The assumptions used in the analysis and the equations for the computation of the stability characteristics of the approximate solutions are also discussed.

### Assumptions

The nonlinear equations of motion used in the calculation of time history responses are the same as those used in reference 11 except that they are

written with respect to principal axes and it is assumed that speed is constant and that sideslip angle is small. Air density is assumed to be constant. The equations are given in appendix A.

To obtain equilibrium, or steady-state, solutions, the equations of appendix A must be solved with all the time derivatives set to zero. This approach was used in reference 11 to calculate equilibrium spin conditions for aircraft. (The computer program used in the study of ref. 11 is described in ref. 12.) The resulting motions calculated in reference 11 consisted of helical paths about a vertical axis. Pseudosteady states (PSS) differ from these truly steady states in that Euler-angle variations which determine the weight-component variations with respect to the body axes are ignored. This approximation is appropriate in analyzing rotational coupling effects in rapid maneuvers because it removes the constraint that the motion be about the vertical axis. This was achieved in the present analysis by ignoring the $\dot{\theta}$ and $\dot{\phi}$ equations of appendix A and by assuming that $\theta = \alpha$ ($\gamma = 0$) and $\phi = 0$ in the $\dot{\alpha}$ and $\dot{\beta}$ equations. The PSS analysis also ignores the $\dot{V}$ equation of reference 11 by assuming that a constant equilibrium cruise velocity is maintained. (Modifications to the assumptions of constant velocity, $\theta = \alpha$, and $\phi = 0$ are made in a later section of the report which gives comparisons between PSS solutions and true equilibrium spin conditions.) The resulting five equations, with their time derivatives set to zero, are used in the following analysis to obtain PSS solutions for any combination of control inputs. The basic assumptions of the PSS method of analysis are (1) that important qualitative dynamic characteristics of rapid aircraft maneuvers can be obtained by studying the state-space loci and stability properties of the approximate equilibrium solutions over the range of practical control combinations and (2) that critical control combinations can be identified by significant changes in the patterns of the state-space loci.

## Solution for Pseudosteady States

Equations (A1) to (A5) of appendix A could be solved for steady states using an optimization algorithm such as that used in reference 11 to compute equilibrium spin conditions. The method of reference 11 required a five-parameter search. The simpler PSS formulation permits reduction of the problem to a two-parameter search, so that it is possible to develop the following simple and efficient PSS solution procedure.

Equations (A1) to (A5) can be written as

$$\bar{p}\bar{q} - \bar{\beta}\hat{n}_\beta - \bar{r}\hat{n}_r = \hat{n}_0 + \bar{p}\hat{n}_p \tag{1}$$

$$\bar{q}\hat{m}_q + \bar{p}\bar{r} = -\hat{m}_0 \tag{2}$$

$$\bar{r}(\cos \bar{\alpha} - Y_r) - \bar{\beta}Y_\beta = Y_0 + (Y_p + \sin \bar{\alpha})\bar{p} \tag{3}$$

8

$$\bar{\beta}\hat{l}_\beta + \bar{p}\hat{l}_p + \bar{r}\hat{l}_r + \hat{l}_0 = \bar{q}\bar{r} \tag{4}$$

$$\bar{q} - \bar{\beta}(\bar{p}\cos\bar{\alpha} + \bar{r}\sin\bar{\alpha}) + Z_0 + g/V = 0 \tag{5}$$

The overbars in the preceding equations indicate PSS solutions and, for convenience, the arguments for the aerodynamic coefficients have been dropped.

Equations (1), (2), and (3) are linear in $\bar{q}$, $\bar{\beta}$, and $\bar{r}$ and can be solved for these variables as functions of $\bar{p}$, $\bar{\alpha}$, and control inputs. These equations can be written in matrix form as follows:

$$\begin{bmatrix} \bar{p} & -\hat{n}_r & -\hat{n}_\beta \\ \hat{m}_q & \bar{p} & 0 \\ 0 & \cos\bar{\alpha} - Y_r & -Y_\beta \end{bmatrix} \begin{bmatrix} \bar{q} \\ \bar{r} \\ \bar{\beta} \end{bmatrix} = \begin{bmatrix} \hat{n}_0 \\ -\hat{m}_0 \\ Y_0 \end{bmatrix} + \bar{p} \begin{bmatrix} \hat{n}_p \\ 0 \\ Y_p + \sin\bar{\alpha} \end{bmatrix} \tag{6}$$

The determinant of the preceding matrix is given by

$$\Delta = D_2\bar{p}^2 + D_0 \tag{7}$$

where

$$D_2 = -Y_\beta$$

$$D_0 = -\hat{m}_q[Y_\beta\hat{n}_r + \hat{n}_\beta(\cos\bar{\alpha} - Y_r)]$$

Solutions for $\bar{q}$, $\bar{r}$, and $\bar{\beta}$ are as follows:

$$\bar{q} = (Q_2\bar{p}^2 + Q_1\bar{p} + Q_0)/\Delta \tag{8}$$

$$\bar{r} = (R_1\bar{p} + R_0)/\Delta \tag{9}$$

$$\bar{\beta} = (B_3\bar{p}^3 + B_2\bar{p}^2 + B_1\bar{p} + B_0)/\Delta \tag{10}$$

9

where

$$Q_2 = \hat{n}_\beta(Y_p + \sin \bar{\alpha}) - Y_\beta \hat{n}_p$$

$$Q_1 = \hat{n}_\beta Y_0 - \hat{n}_0 Y_\beta$$

$$Q_0 = \hat{m}_0 [Y_\beta \hat{n}_r + \hat{n}_\beta(\cos \bar{\alpha} - Y_r)]$$

$$R_1 = \hat{m}_0 Y_\beta - \hat{m}_q [\hat{n}_\beta(Y_p + \sin \bar{\alpha}) - Y_\beta \hat{n}_p]$$

$$R_0 = \hat{m}_q(\hat{n}_0 Y_\beta - \hat{n}_\beta Y_0)$$

$$B_3 = Y_p + \sin \bar{\alpha}$$

$$B_2 = Y_0$$

$$B_1 = (\cos \bar{\alpha} - Y_r)(\hat{m}_0 - \hat{m}_q \hat{n}_p) + \hat{m}_q \hat{n}_r(Y_p + \sin \bar{\alpha})$$

$$B_0 = \hat{m}_q [\hat{n}_r Y_0 + \hat{n}_0(\cos \bar{\alpha} - Y_r)]$$

Substituting these values for $\bar{q}$, $r$, and $\bar{\beta}$ into equation (4) gives the following polynomial in $\bar{p}$:

$$A_5 \bar{p}^5 + A_4 \bar{p}^4 + A_3 \bar{p}^3 + A_2 \bar{p}^2 + A_1 \bar{p} + A_0 = 0 \tag{11}$$

where

$$A_5 = D_2(\hat{l}_\beta B_3 + \hat{l}_p D_2)$$

$$A_4 = D_2(\hat{l}_\beta B_2 + \hat{l}_0 D_2)$$

$$A_3 = \hat{l}_\beta(D_0 B_3 + D_2 B_1) + D_2(\hat{l}_r R_1 + 2\hat{l}_p D_0) - Q_2 R_1$$

$$A_2 = \hat{l}_\beta(D_0 B_2 + D_2 B_0) + R_0(\hat{l}_r D_2 - Q_2) + 2\hat{l}_0 D_0 D_2 - Q_1 R_1$$

$$A_1 = D_0(\hat{l}_\beta B_1 - \hat{l}_r R_1) - Q_1 R_0 - Q_0 R_1 + \hat{l}_p D_0{}^2$$

$$A_0 = D_0(\hat{l}_\beta B_0 + \hat{l}_r R_0 + \hat{l}_0 D_0) - Q_0 R_0$$

Simultaneous solution of equations (5) and (11) yields PSS values for $\bar{p}$, $\bar{\alpha}$, $\bar{q}$, $\bar{r}$, and $\bar{\beta}$ for specified values of the control inputs. (Eqs. (8), (9), and (10) are used to compute $\bar{q}$, $\bar{r}$, and $\bar{\beta}$.) Various iterative search algorithms could be used to solve equations (5) and (11). The search procedure employed in the present study is described in appendix B.

## Stability of PSS Solutions

The stability of any particular set of PSS solutions was calculated by linearizing the first five equations of appendix A about the PSS solution. The matrix whose characteristic roots determine the stability of a perturbed motion is given by

$$
\begin{bmatrix}
n_r & -J_Z\bar{p} & n_\beta & n_p - J_Z\bar{q} & \dot{r}_\alpha \\
J_Y\bar{p} & m_q & 0 & J_Y\bar{r} & \dot{q}_\alpha \\
Y_r - \cos\bar{\alpha} & 0 & Y_\beta & Y_p + \sin\bar{\alpha} & \dot{\beta}_\alpha \\
l_r - J_X\bar{q} & -J_X\bar{r} & l_\beta & l_p & \dot{p}_\alpha \\
-\bar{\beta}\sin\bar{\alpha} & 1 & -\bar{p}\cos\bar{\alpha} - \bar{r}\sin\bar{\alpha} & -\bar{\beta}\cos\bar{\alpha} & \dot{\alpha}_\alpha
\end{bmatrix}
= [A] \qquad (12)
$$

where

$$\dot{r}_\alpha = n_{\beta_\alpha}\bar{\beta} + n_{p_\alpha}\bar{p} + n_{r_\alpha}\bar{r} + n_{0_\alpha}$$

$$\dot{q}_\alpha = m_{q_\alpha}\bar{q} + m_{0_\alpha}$$

$$\dot{\beta}_\alpha = \bar{r}\sin\bar{\alpha} + \bar{p}\cos\bar{\alpha} + Y_{\beta_\alpha}\bar{\beta} + Y_{p_\alpha}\bar{p} + Y_{r_\alpha}\bar{r} + Y_{0_\alpha}$$

$$\dot{p}_\alpha = l_{\beta_\alpha}\bar{\beta} + l_{p_\alpha}\bar{p} + l_{r_\alpha}\bar{r} + l_{0_\alpha}$$

$$\dot{\alpha}_\alpha = \bar{p}\bar{\beta}\sin\bar{\alpha} - \bar{r}\bar{\beta}\cos\bar{\alpha} + Z_{0_\alpha}$$

In the preceding equations, the absence of carets (^) on the moment derivatives indicates that the inertia ratios are not factored out as in the equations of appendix A.

It should be noted that the stability characteristics as defined by [A] are approximate, since the varying weight components (in the $\dot{\alpha}$ and $\dot{\beta}$ equations of appendix A) are neglected. Also, stability derivatives in column 5 of [A] were computed by taking numerical slopes using linear interpolation on the nonlinear aerodynamic data. This procedure introduces discontinuities in the stability derivatives at breakpoints in the tabular aerodynamic data used in the computer program. However, these approximate stability characteristics are considered adequate for the present analysis since the PSS solutions are only approximate steady states.

## DESCRIPTION OF AIRCRAFT CONFIGURATION

The assumed aircraft of the present study is representative of a twin-jet, swept-wing fighter. The aircraft was assumed to be flying at an altitude of 13 720 m and at a Mach number of 0.9 (V = 266 m/sec, $q_\infty$ = 8400 Pa). It should be noted that this flight condition is more representative of a flight test condition than of normal operational flight.

Weight, inertia, and dimensional characteristics for the aircraft are given in table I. Aerodynamic data used in the analysis were taken from references 13 and 14 and are tabulated in table II. With the exception of $C_{l_\beta}$, $C_{n_\beta}$, and $C_{Y_\beta}$, the $\beta = 0$ data of reference 13 were used to represent the coefficients. The coefficients $C_{l_\beta}$, $C_{n_\beta}$, and $C_{Y_\beta}$ were determined at each angle of attack by taking the slope of the data of reference 13 between side-slip angles of $\pm 5^\circ$. (It should be noted that the assumption of linearity in $\beta$ can introduce errors in time history responses which involve large transient motions in sideslip angle.) The dynamic stability derivatives were taken from reference 14. Linear interpolation was used between the data points given in table II. Variations of several important lateral-directional parameters with $\alpha$ are given on figure 1. These include $C_{n_\beta}$, $C_{l_\beta}$, and two parameters which

are strongly dependent on these - $C_{n_\beta,dyn}$, which is commonly used as an indica-

tor of divergence tendency, and $E_a$, which is an approximate measure of aileron roll effectiveness.

## RESULTS AND DISCUSSION

The pseudosteady-state (PSS) method has been applied to a number of maneuvers for the assumed aircraft. These included aileron roll maneuvers about a one-g condition (Lift = Weight, Pitching moment = 0) and roll maneuvers initiated from pitch-up (Acceleration > g) and pitch-down (Acceleration < g) conditions. The trim conditions considered in the analysis are summarized in table III. PSS predictions for the aforementioned maneuvers are now discussed. Time history responses are then presented to validate the PSS predictions.

## PSS Solutions

PSS solutions for angle of attack, roll rate, yaw rate, sideslip angle, and pitch rate for various aileron inputs are shown on figure 2 for the one-g trim condition. (The one-g condition actually required $\delta_e = -3.1°$, which is hereafter referred to as $\Delta\delta_e = 0°$; all other elevator settings are given as increments from the one-g condition.) Figure 2(a) shows angle-of-attack solutions. The curves are numbered from 1 to 6 in order of increasing angle of attack. The curves are also labeled as P or N to indicate positive or negative roll rates, as shown on figure 2(b). The stability of the solutions is indicated on the figure; the stability characteristics are tabulated in table IV for selected aileron inputs. Consider the $\delta_a = -25°$ results of table IV for the 2P and 3P curves. Figure 2 shows that the values for $\bar{p}$, $\bar{\alpha}$, $\bar{\beta}$, $\bar{q}$, and $\bar{r}$ are approximately the same at this condition. Therefore, we would expect the characteristic roots to be approximately the same for $\delta_a = -25°$ on the 2P and 3P curves. The differences shown in table IV result from the previously mentioned method for finding the stability derivatives in column 5 of [A] since 2P and 3P are on opposite sides of a breakpoint in the tabular aerodynamic data at $\alpha = 35°$. (Column 5 of [A] was computed by taking numerical slopes using linear interpolation between data points. This procedure introduces discontinuities at breakpoints in the tabular aerodynamic data.) If a more accurate stability representation is desired, a higher order interpolation scheme should be used in fitting the aerodynamic data.

Figure 2 shows that there are multiple PSS solutions for all aileron settings. As shown in previous studies (refs. 7 and 8), the existence of multiple PSS solutions can lead in various ways to predictions of a divergence in response at certain control input combinations. Divergences are associated with the behavior of the basic solution, that being the normal aircraft response curve (curve 1, fig. 2) starting at $p = 0$ and $\delta_a = 0$. If the basic solution disappears at some control combinations by joining another solution (curves 2 and 3 join on fig. 2), then the response would be expected to diverge to the vicinity of another PSS solution. Also, if the basic solution comes close in state space to another solution, a perturbed response may enter the domain of attraction of the other solution and a divergence might occur.

The stability of the PSS solutions is important in determining possible attractor states. Solid lines on figure 2 represent stable solutions which are strong attractors. Short dashed lines represent solutions for which a divergence would occur. Short-long dashed lines are potential attractors since they indicate an unstable oscillation. Of course, the regime of each PSS solution has a significant effect on the aircraft response when a maneuver enters that regime depending on the stability properties in its domain of influence. For example, if the maneuver enters the domain of influence of a strongly divergent solution, the response should rapidly diverge to a more stable regime.

We now analyze figure 2 with respect to possible divergences in aircraft response. Since the basic solution for $\Delta\delta_e = 0$ remains stable for all aileron deflections, the only possibility of a divergence would be for the basic solution curve to enter the domain of attraction of other curves. This occurs for large aileron inputs in the roll-rate solution for curves 4P, 5P, and 6P (fig. 2(b)). However, the basic solution is far away from the other 4P, 5P,

and 6P solutions of figure 2, particularly the angle-of-attack solutions. Since angle of attack is such an important parameter in determining the response characteristics with nonlinear aerodynamics, a divergence would be unlikely; that is, the aircraft response would be expected to attain the levels of the basic solution for all aileron inputs. Nevertheless, there is enough uncertainty in this case that the conclusion is verified with time history responses.

The high-angle-of-attack solutions ($\alpha > 25^O$) of figure 2 are of interest since they resemble possible spin conditions ($\alpha$ above stall, large rotation rates). These solutions, which are typical of those obtained with other elevator inputs, are discussed in some detail in a later section of the report. However, for the present, only the PSS solutions in the normal operational envelope ($\alpha < 25^O$) of the aircraft are considered.

Figure 3 shows PSS solutions for roll rate, sideslip angle, angle of attack, pitch rate, and yaw rate as a function of aileron deflection for various elevator increments above and below the one-g trim value ($\Delta\delta_e = 0^O$). Only the basic solution curves and those associated with the basic solution are given on figure 3. No solutions for angles of attack greater than $25^O$ are shown. The stability characteristics at various points on the curves of figure 3 are given in table V.

Consider the one-g ($\Delta\delta_e = 0$) solution. Figure 3(a) shows that as aileron deflection is increased, roll rate begins to saturate; that is, the increasing positive sideslip angle (fig. 3(b)) acts through $C_{l_\beta}$ to reduce roll rate. This effect is even more evident for the pitch-up maneuvers with $\Delta\delta_e = -4^O$ and $-8^O$. At the high angle of attack corresponding to $\Delta\delta_e = -8^O$ (fig. 3(c)), the aileron effectiveness in producing roll almost vanishes and at $\Delta\delta_e = -12^O$, a roll reversal occurs (negative aileron deflection generally gives positive roll rate). This is predicted by the aileron effectiveness results of figure 1 which show a reversal in effectiveness for angles of attack greater than about $20^O$.

Now consider the pitch-down ($\Delta\delta_e > 0^O$) rolling maneuvers shown on figure 3. For $\Delta\delta_e = 6^O$ and $8^O$, there are multiple PSS values for certain aileron inputs. For these cases, as aileron deflection increases beyond a certain level, the basic solution disappears by joining a divergent PSS solution. For aileron inputs greater than the value at which the basic solution disappears, the aircraft response would be expected to diverge to the vicinity of other stable PSS solutions.

Consider the PSS solutions for $\Delta\delta_e = 8^O$ shown on figure 3. This case corresponds to rolling maneuvers about a -0.6g condition. For aileron inputs up to about $-9^O$, the steady-state response would be expected to reach the levels of the basic solution. As the aileron deflection is increased from $-9^O$ to about $-10^O$, the following would be expected to happen. The roll rate (fig. 3(a)) would jump from about 70 deg/sec to about 145 deg/sec; angle of attack (fig. 3(c)), from about $-6^O$ to about $7.5^O$; and yaw rate (fig. 3(e)), from about $-8^O$ deg/sec to about 20 deg/sec. The steady-state values for sideslip angle and pitch rate (figs. 3(b) and 3(d)) would be about the same as before the divergence. Similar predictions could be made for $\Delta\delta_e = 6^O$ on figure 3.

The roll-rate response predictions of figure 3(a) for $\Delta\delta_e = 4^O$ are interesting. This case, which corresponds to rolls about a nearly zero-g condition, is the approximate boundary between different types of coupled responses. Figure 3(a) shows that for aileron deflections up to about $-26^O$, the roll rate appears to be saturating. However, for even small increases in aileron deflection above $-26^O$, the roll response increases rapidly. This roll response was predicted by the analysis of reference 1. That analysis predicted an unstable aircraft response if the roll-rate magnitude was between the values for the undamped natural frequencies of the longitudinal and lateral modes of the aircraft. The longitudinal and lateral frequencies are approximately $(-\hat{m}_{0\alpha})^{1/2}$ and $(\hat{n}_\beta)^{1/2}$, respectively. For $\Delta\delta_e = 4^O$, and $\delta_a = -26^O$ on figure 3, the longitudinal and lateral frequencies are approximately equal, both being about 125 deg/sec.

In contrast to the pitch-down elevator responses just discussed, consider the other extreme, $\Delta\delta_e = -12^O$ on figure 3. This case corresponds to rolls about a 2.2g pitch-up condition. For small aileron inputs, there is a reversal in aileron effectiveness and the basic solution shows an unstable oscillation. For aileron deflections greater than about $-1.5^O$, the basic solution disappears and figure 3 shows that there are no other solutions for the angle-of-attack range shown. For all aileron inputs, there are, however, several high-angle-of-attack solutions similar to those shown on figure 2. Thus, even for small aileron inputs, we would expect the $\Delta\delta_e = -12^O$ response to diverge toward the high-angle-of-attack PSS solutions.

## Summary of PSS Solutions

Three types of maneuvers were analyzed in the previous discussion. These included rolls about a one-g trim condition and rolling maneuvers using pitch-down and pitch-up elevator deflections. Figure 4 illustrates the general nature of the PSS solutions for these three types of maneuvers and the possible problems associated with each. The circled numbers represent the different solution types, ordered by increasing angle of attack, as on figure 2. Shown on figure 4(a) are all positive roll-rate solutions for the combinations of $\Delta\delta_e$ and $\delta_a$ given on figure 3. Showing the solutions as a function of angle of attack gives a better understanding of the relationship between various solutions. The stability characteristics of the solutions are also shown. Negative roll-rate solutions would be a mirror image of the positive solutions shown on figure 4(a); that is, the positive curves of figure 4(a) could be rotated about the $\bar{p} = 0$ axis to become negative solutions, in which case the sign of the aileron deflection would be reversed.

Consider the pitch-down ($\Delta\delta_e > 0$) cases shown on figure 4(a). For $\Delta\delta_e = 6^O$ and $8^O$, the basic solution disappears at some critical aileron input. For aileron deflections greater than these critical values the response could be expected to diverge to the high-roll rate, low-angle-of-attack solutions in the upper left-hand part of figure 4. This region is a spin stabilized region, where gyroscopic momentum adds to the "stiffness" in $\alpha$ and $\beta$. There is a possibility that the response would be attracted to the high-angle-of-attack solutions once the basic solution vanishes. This possibility is investigated with time history calculations in a later section.

Now consider the basic solution (1) curves of figure 4(a) for pitch-up maneuvers ($\Delta\delta_e < 0$). The previously shown roll-rate saturation with increasing aileron deflection is evident. Also evident is the reduced aileron effectiveness as pitch-up elevator deflection ($-\Delta\delta_e$) is increased. That is, as the trim angle of attack corresponding to pitch-up elevator deflection increases, the roll effectiveness of the aileron decreases. As shown on figure 4(a), aileron effectiveness becomes zero and then reverses for angles of attack above about $20^\circ$. The reversal is not caused by a change in sign of $C_{l_{\delta_a}}$, but results from a

change in sign of the aileron effectiveness parameter shown on figure 1. The roll reversal is clearly seen for $\Delta\delta_e = -12^\circ$ on figure 4(a). For this case the basic solution joins a divergent solution for aileron deflections greater than about $1.5^\circ$ in magnitude and, for larger aileron deflections, the only attractors are solutions 3, 4, 5, and 6, which have angles of attack greater than about $25^\circ$. This suggests that for this case, the aircraft response would diverge to high angles of attack for aileron inputs greater than about $1.5^\circ$ in magnitude.

The high-angle-of-attack, spinlike regimes are better illustrated by showing total angular velocity as a function of angle of attack. This is shown on figure 4(b) for the range of $\Delta\delta_e$ and $\delta_a$ given on figure 4(a). For the curves shown on figure 4(b), angular velocity is composed almost entirely of $p$ and $r$ with the $q$ contribution being insignificant.

A comparison of figure 4(b) with 4(a) shows that for angles of attack up to about $25^\circ$, angular velocity is dominated by roll rate. For $\alpha > 25^\circ$, there is a gradual increase in yaw rate, and at about $\alpha = 45^\circ$, the $p$ and $r$ contributions to angular velocity are about equal. For higher angles of attack, yaw rate is the dominant term in the angular velocity. The 5- and 6-type solutions shown on figure 4(b) are composed almost entirely of yaw rate.

The divergent 2-type curves shown on figure 4 may represent the spin departure region since the aircraft response would be expected to diverge rapidly through this region. The oscillatory 3-type and divergent 4-type curves resemble steep and intermediate spin conditions. The oscillatory 5-type and divergent 6-type solutions may represent flat spin conditions. We refer to these as spin conditions, although if the aerodynamic representation were accurate, one would not expect the aircraft to spin at a condition which is predicted to be divergent. It should also be noted that assuming the velocity to be the constant cruise value is invalid at high angles of attack. This is discussed in a later section of the report.

In summary, figure 4 shows that depending on the control combinations, the aircraft response can be attracted to three distinct regions. It can remain at low angles of attack and moderate roll rates, it can diverge to low angles of attack and high roll rates, or it may diverge to high angles of attack and large rotation rates.

## Time History Responses

Time history responses are now presented to validate the PSS predictions of figures 3 and 4. Responses are given for maneuvers about a one-g trim condition, pitch-down conditions, and pitch-up conditions. While the PSS analyis neglected the varying gravity components, the time histories were calculated using the complete equations of motion given in appendix A, unless otherwise noted.

One-g trim maneuvers.- Time history calculations for rolling maneuvers about the one-g trim condition ($\Delta\delta_e = 0$) agreed well with the PSS predictions of figure 3. At any aileron deflection, the steady-state value for all variables was close to that predicted by the basic solution of figure 3. Roll-rate and sideslip-angle responses are shown on figure 5 for two aileron inputs. PSS predictions are also noted. As can be seen, the responses are close to the PSS predictions. Similar agreement was found for the other variables. One of the roots predicted by the stability characteristics of table V is evident in the time histories of figure 5. A mode having a root with a period of 2.8 seconds was predicted for $\delta_a = -5^O$. The corresponding $p$ and $\beta$ histories have a period of about 3 seconds. A mode having a root with a period of 2.1 seconds was predicted for $\delta_a = -30^O$. The corresponding $p$ and $\beta$ histories contain an oscillation with a period of about 2 seconds.

Pitch-down maneuvers.- Time history responses for pitch-down elevator deflections ($\Delta\delta_e > 0^O$) were in agreement with the PSS predictions of figures 3 and 4. For example, for $\Delta\delta_e = 8^O$, figure 3 predicts a divergence for an aileron input of about $-9.5^O$. Time history responses showed that the divergence actually occurs for aileron deflections of $-10^O$ or greater.

Figure 6 illustrates the aircraft response before and after a coupled divergence for the $\Delta\delta_e = 8^O$ maneuver. For this case, which is typical of coupled responses, aileron deflection was maintained at $-8^O$ for the first 5 seconds and then increased to $-12^O$. PSS predictions for each aileron deflection are also indicated on figure 6. The roll-rate, pitch-rate, yaw-rate, angle-of-attack, and sideslip-angle responses at 5 seconds are in general agreement with the PSS basic solution of figure 3 for $\delta_a = -8^O$. When the aileron deflection is increased to $-12^O$ after 5 seconds, the tendency to diverge is evident first in $p$ and $\beta$. The increasing negative sideslip acts through the dihedral effect $C_{l_\beta}$ to accelerate the rolling. At about 13 seconds the coupling terms in the $\dot{r}$ and $\dot{\alpha}$ equations (appendix A), that is the $-pq$ and $-p\beta \cos \alpha$ terms, cause $r$ and $\alpha$ to diverge toward the positive values predicted on figures 3(e) and 3(c). At about 16 seconds, a similar coupled divergence occurs in pitch rate (caused by the $pr$ term in the $\dot{q}$ equation). An interesting feature of the responses shown on figure 6 is that all the variables initially diverge toward values consistent with the divergent autorotational values ($\Delta\delta_e = 8^O$, $\delta_a = 0^O$) shown on figure 3. It appears that the transition between the two stable conditions is characterized by a passage through the divergent $\Delta\delta_e = 8^O$ and $\delta_a = 0^O$ domain.

The major factors contributing to the effects shown on figure 6 are given on figure 7. Shown are the dominant terms in the $\dot{p}$, $\dot{r}$, and $\dot{\beta}$ equations. The $\dot{\beta}$ components given on figure 7(a) show that the divergence to negative sideslip angles shown on figure 6 is caused by the $p \sin \alpha$ coupling term. Consider the components of the roll acceleration shown on figure 7(b). As can be seen, $\hat{l}_\beta$ in combination with the applied rolling moment ($l_0$), overcomes the damping in roll ($l_p$) to increase the roll acceleration. The $qr$ coupling term, which is not shown has an insignificant effect on $\dot{p}$. In contrast, the coupling term $-pq$ in the yaw-acceleration response of figure 7(c) is the driving term. Similar roll coupled effects occur in the $\dot{q}$ and $\dot{\alpha}$ equations because of $pr$ and $p\beta \cos \alpha$.

While the initial rapid divergence associated with rotational coupling is the important aspect of the present analysis, it is of interest to check the PSS predictions following a divergence. Continuation of time histories of figure 6 beyond 20 seconds would show the responses converging to values near the PSS predictions. This is illustrated better by using an aileron deflection further removed from the critical value of about $-10^o$. Shown on figure 8 are $p$, $\alpha$, and $r$ responses for $\Delta\delta_e = 8^o$ and $\delta_a = -15^o$. As shown, the responses after divergence are close to the PSS predictions of figure 3.

Suppose that a time history is initiated at PSS values corresponding to the $\Delta\delta_e = 8^o$ and $\delta_a = -15^o$ condition of figure 3 and that the aileron deflection is then reduced to zero. The results of figure 3 suggest that the aircraft states would not return to their trim values (table III) but would remain at their autorotational values. For example, roll rate might be expected not to return to zero but to attain the autorotational, $\delta_a = 0^o$ value of about 140 deg/sec shown on figure 3(a). The responses are attracted to the autorotational values if the aileron is ramped back to zero at a rate of about 5 deg/sec or less. Figure 9 shows two roll-rate responses initiated from the $\Delta\delta_e = 8^o$, $\delta\alpha = -15^o$, PSS condition for which the aileron deflection was ramped down to zero at a rate of 5 deg/sec. The responses were calculated both with and without the varying weight components as shown on the figure. Both responses are attracted to the autorotational, PSS solution.

However, when the aileron deflection was immediately set at zero, the variables returned to the levels of the trim condition after about 6 seconds. This is because of the inclusion in the time history calculations of varying weight components which were omitted in the PSS analysis. When the weight-component variations were omitted from the time history calculations ($\dot{\phi} = \dot{\theta} = 0$) and $\delta_a$ was set immediately to zero, the responses continued to oscillate about the autorotational values.

Pitch-up maneuvers.- Time history calculations were in agreement with the PSS predictions of figure 3 for $\Delta\delta_e = -4^o$ and $-8^o$. The steady-state values for all variables attained the level of the PSS predictions for all aileron inputs with no tendency to diverge.

Now consider the results shown on figure 3 for $\Delta\delta_e = -12^o$. The low roll rates associated with this maneuver are not of the type for which the analysis was intended. However, the maneuver is of interest since the results of fig-

ures 3 and 4 predicted roll reversal for the basic solution and a divergence to high angles of attack and large rotation rates for small aileron deflections.

Time history responses verified the PSS predictions for $\Delta\delta_e = -12^O$. For all aileron deflections, the response initially diverged to the vicinity of the high-angle-of-attack PSS predictions. This behavior is illustrated on figure 10. Shown are $p$, $\alpha$, $\beta$, $q$, and $r$ time histories for an aileron deflection of $-5^O$. This response is typical of those for other aileron deflections. The figure shows that during the first 3 seconds, $\alpha$, $\beta$, and $r$ gradually increase in magnitude. At a time of about 3 seconds, there is a rapid divergence in all response variables. Continuation of the time history beyond 5 seconds shows the response approximately repeating the history shown on figure 10 between about 3 to 5 seconds, with $p$ and $r$ oscillating between large positive and negative values.

The initial divergence shown on figure 10 is caused by both aerodynamic and coupling effects and can be understood by examining the component parts of the equations of appendix A. The dominant components of the $\dot{\beta}$, $\dot{r}$, and $\dot{p}$ equations are shown on figure 11. Figure 11(a) shows that the increasing sideslip angle is caused by the $r\cos\alpha$ coupling term, while figure 11(b) shows that the unstable $\hat{n}_\beta$ causes yaw accelerations to diverge to negative values. That is, $C_{n_\beta}$ becomes negative for angles of attack greater than about $22^O$ (fig. 1) and acts through $\beta\hat{n}_\beta$ to increase the magnitude of yaw rate. This is reflected in the stability predictions of table V which show unstable oscillatory roots for $\Delta\delta_e = -12^O$.

The components of the rolling-moment equation are shown on figure 11(c). For about the first 3 seconds $r\hat{l}_r$, $\beta\hat{l}_\beta$, and $\hat{l}_0$ nearly balance each other to result in a small negative roll rate. At slightly less than 3 seconds, the dihedral effect $C_{l_\beta}$ causes roll acceleration to diverge to large negative values. As seen on figure 11(c), $\beta\hat{l}_\beta$ is positive between about 2.2 seconds and 2.9 seconds. Since $\beta$ is positive during this period (fig. 10), $C_{l_\beta}$ must also be positive. This is, in fact, the case between angles of attack of about $25^O$ and $35^O$ as shown on figure 1. When angle of attack exceeds $35^O$ at about 3 seconds, $C_{l_\beta}$ becomes negative and causes roll acceleration to diverge as shown on figure 11(c).

The responses shown on figure 10 for the first 3 seconds are largely due to aerodynamic effects. However, the continuing rapid oscillations after 3 seconds are highly coupled about all aircraft axes.

It should be emphasized that the physically significant portion of the time history of figure 10 is the initial divergence occurring during the first 3 seconds. After that, angle of attack is above the stall and the constant velocity assumption is invalid since velocity would decrease rapidly at high angles of attack. In addition, for large sideslip angles, the linearity assumption in such coefficients as $C_{l_\beta}$ is also invalid. However, it is of academic interest to examine these responses to see how they are influenced by the spinlike PSS solutions obtained in the analysis.

A clearer picture of how the response of figure 10 is attracted to the high-angle-of-attack solutions is obtained by showing $p$ and $\alpha$, $r$ and $\alpha$,

and $\omega$ and $\alpha$ phase plots for the time history of figure 10. The first 9 seconds of these trajectories is given on figure 12. Also shown are the PSS predictions. The predictions are numbered 2 through 6 in accordance with the notation of figure 4 and the stability of the predictions is also indicated. Consider the p and $\alpha$ and r and $\alpha$ responses shown on figures 12(a) and 12(b). Initially the motion seems to be attracted toward PSS solutions 3 and 4. Then there is a rapid divergence toward solutions 5 and 6, followed by a return to the lower-angle-of-attack region. For the remainder of the trajectory, both responses are in the domain of influence of solutions 2, 3, and 4. The $\omega$ and $\alpha$ response shown on figure 12(c) follows a pattern similar to these, except that it initally passses through the divergent solution 2. Continuation beyond 9 seconds shows the responses repeating similar patterns in p and $\alpha$, r and $\alpha$, and $\omega$ and $\alpha$ space.

## Comparison of PSS Solutions With Equilibrium Spin Conditions

As previously shown on figures 2 and 4, PSS solutions which occur at high angles of attack resemble possible spin conditions in that they involve high rotation rates. Consider again the results of figure 4. The divergent 2-type curves may represent the spin departure region through which the aircraft response would be expected to diverge rapidly. The oscillatory 3-type solutions resemble steep spin conditions while the divergent 4-type solutions may represent intermediate spin conditions. The oscillatory 5-type and divergent 6-type solutions resemble flat spin conditions. Comparisons are now made between PSS solutions and equilibrium spin solutions obtained using the method of reference 11. Before making these comparisons, the following points should be emphasized. In the method of reference 11, the motion occurs in a helical path about the vertical. In addition, all seven equations of appendix A, along with the equation for rate of change of velocity, are used in the method of reference 11. In brief, the method uses a minimization algorithm to find those combinations of trajectory variables for which all time derivatives of the equations of motion vanish.

The PSS analysis neglects weight-component variation effects, so that pseudosteady-state solutions other than helical motions about a vertical axis are permitted. In a truly steady motion, such as an equilibrium spin, $\theta$ and $\phi$ are fixed. Therefore it is reasonable to expect that approximate spin solutions may be found by the PSS analysis, since in the true spin the weight components are constant, even though changed from PSS values because $\theta \neq \alpha$ and $\phi \neq 0$. Also, the moment balance in which the weight plays no role is more important than the force balance in a spin.

The PSS analysis shown up to this point assumes constant velocity regardless of angle of attack. In a true equilibrium spin, velocity decreases rapidly as angle of attack increases above the stall. A good approximation of the true velocity in a spin can be obtained by calculating the velocity for which the drag is equal to the aircraft weight. In a true equilibrium spin, $\theta$ is not equal to $\alpha$ ($\gamma \neq 0$) as was assumed in the PSS analysis. A reasonable approximation would be to assume that $\gamma = -90^\circ$ ($\theta - \alpha = -90^\circ$) and $\phi = \beta$ at high angles of attack.

An additional point which should be emphasized is that the aerodynamic representation of this report may be unrealistic for investigating spinning conditions. Numerous studies (ref. 15, for example) have shown that a more realistic representation would be for the aerodynamic data to be functions not only of $\alpha$ and $\beta$, but also of spin rate. However, as was shown in reference 11, aerodynamic data of the form used in the present study can give reasonable predictions of true equilibrium spin conditions for fighter-type aircraft.

A comparison of high-angle-of-attack PSS solutions with equilibrium spin solutions is given in table VI for the one-g, $\delta_a = 0$ condition. These results are typical of those obtained with other control deflections. Shown in table VI are the predictions using the method of reference 11 including the eighth order stability characteristics. Also shown are three sets of PSS predictions and their fifth order stability characteristics. PSS solutions were first calculated by assuming that Mach number was 0.9, $\theta = \alpha$, and $\phi = 0$. They were then calculated using the velocity for which the aircraft drag was equal to the weight (D = W) with $\theta = \alpha$ and $\phi = 0$. The final PSS calculation assumed that D = W, $\phi = \beta$, and $\gamma = -90^{\circ}$ ($\theta - \alpha = -90^{\circ}$). An examination of the $\dot{\alpha}$ and $\dot{\beta}$ equations of appendix A shows that assuming $\phi = \beta$ and $\gamma = -90^{\circ}$ eliminates the g/V term in the $\dot{\alpha}$ equation (for small $\beta$) and introduces a $(g/V)(\sin \bar{\alpha} - 1)\beta$ term in the $\dot{\beta}$ equation. This was implemented in the PSS analysis by replacing $Y_\beta$ in equation (3) with $Y_\beta - g/V(\sin \bar{\alpha} - 1)$ and setting g/V to zero in equation (5). As shown in table VI, both methods yield four high-angle-of-attack solutions. For the lowest and two highest angles of attack, there is reasonable agreement between the predicted values of the variables when the velocity corresponding to D = W is used. A slight additional improvement is obtained using D = W and $\gamma = -90^{\circ}$. The PSS predictions of table VI for the intermediate spin at an angle of attack of about $60^{\circ}$ are not in as good agreement with significant variations occurring in all variables. The fifth and eighth order stability predictions shown in table VI follow similar trends in all cases. The results of table VI suggest that the high-angle-of-attack solutions obtained in the PSS analysis are reasonable approximations to the equilibrium spin conditions obtained using the method of reference 11.

## CONCLUDING REMARKS

A pseudosteady-state (PSS) method was presented for studying the combined effects of rotational coupling and nonlinear aerodynamics on aircraft response. The method involves the simultaneous solution of two nonlinear equations which are functions of angle of attack, roll rate, and control inputs. Emphasis was placed on the physical and engineering interpretation of the method and results, with a minimum of mathematical sophistication.

The method was applied to a number of pitch and roll maneuvers for a fighter-type aircraft. Included were aileron rolls initiated from a one-g trim condition, pitch-down elevator conditions, and pitch-up elevator conditions.

For pitch-down rolling maneuvers, divergence was found to occur for moderate aileron inputs. The resulting response was attracted to a stable PSS regime

characterized by high roll rate and low angles of attack and sideslip. For pitch-up rolling maneuvers the dominant effects were the degradation of lateral stability and control characteristics at high angles of attack. The combination of roll reversal and lateral divergence resulted in large, irregular, highly coupled responses. For example, for certain combinations of pitch-up elevator and aileron deflections, it was shown that there were no stable PSS solutions, and the resulting violent motions could be qualitatively understood as a cyclic transition between neighboring PSS solutions. Very high angles of attack and high rotation rates in this response resulted from the influence of spinlike PSS solutions.

Four spinlike PSS solutions were compared with true equilibrium spin conditions. The steep and two flat spin solutions were shown to correspond well to the exact solutions, whereas the intermediate, divergent solution was less accurate.


Langley Research Center
National Aeronautics and Space Administration
Hampton, VA 23665
October 22, 1980

## APPENDIX A

## EQUATIONS OF MOTION

The equations of motion used in the calculation of time history responses are listed below. The equations are written with respect to principal axes. Speed and air density are assumed to be constant and the sideslip angle is assumed to be small.

$$\dot{r} = J_Z[-pq + \beta \hat{n}_\beta(\alpha) + p \hat{n}_p(\alpha) + r \hat{n}_r(\alpha) + \hat{n}_0(\alpha,\delta_a,\delta_r)] \tag{A1}$$

$$\dot{q} = J_Y[pr + q \hat{m}_q(\alpha) + \hat{m}_0(\alpha,\delta_e)] \tag{A2}$$

$$\dot{\beta} = -r \cos \alpha + p \sin \alpha + \beta Y_\beta(\alpha) + p Y_p(\alpha) + r Y_r(\alpha) + Y_0(\alpha,\delta_a,\delta_r)$$

$$+ \frac{g}{V}[\cos \theta \sin \phi + (\cos \alpha \sin \theta - \sin \alpha \cos \theta \cos \phi)\beta] \tag{A3}$$

$$\dot{p} = J_X[-qr + \beta \hat{l}_\beta(\alpha) + p \hat{l}_p(\alpha) + r \hat{l}_r(\alpha) + \hat{l}_0(\alpha,\delta_a,\delta_r)] \tag{A4}$$

$$\dot{a} = q - \beta(p \cos \alpha + r \sin \alpha) + Z_0(\alpha,\delta_e)$$

$$+ \frac{g}{V}(\cos \alpha \cos \theta \cos \phi + \sin \alpha \sin \theta) \tag{A5}$$

$$\dot{\phi} = p + \tan \theta(q \sin \phi + r \cos \phi) \tag{A6}$$

$$\dot{\theta} = q \cos \phi - r \sin \phi \tag{A7}$$

where

$$\hat{n}_0(\alpha,\delta_a,\delta_r) = \hat{n}_{\delta_a}(\alpha) \delta_a + \hat{n}_{\delta_r}(\alpha) \delta_r$$

$$\hat{m}_0(\alpha,\delta_e) = \hat{m}(\alpha) + \hat{m}_{\delta_e}(\alpha) \delta_e$$

$$Y_0(\alpha,\delta_a,\delta_r) = Y_{\delta_a}(\alpha) \delta_a + Y_{\delta_r}(\alpha) \delta_r$$

23

$$\hat{l}_0(\alpha, \delta_a, \delta_r) = \hat{l}_{\delta_a}(\alpha)\ \delta_a + \hat{l}_{\delta_r}(\alpha)\ \delta_r$$

$$z_0(\alpha, \delta_e) = \left[ z(\alpha) + z_{\delta_e}(\alpha)\ \delta_e \right] \cos\alpha - \left[ x(\alpha) + x_{\delta_e}(\alpha)\ \delta_e \right] \sin\alpha$$

## APPENDIX B

## SOLUTION PROCEDURE

In order to find PSS solutions for $\bar{p}$, $\bar{\alpha}$, $\bar{q}$, $\bar{r}$, and $\bar{\beta}$, it is necessary to obtain a simultaneous solution to equations (5) and (11), given in the section of the text, "Solution for Pseudosteady States." Since the equations are nonlinear, an iterative search procedure employed in the analysis is now described.

For fixed values of the control inputs, angle of attack was increased from $-10^{\circ}$ to $90^{\circ}$ in increments of $0.1^{\circ}$. Solutions to equation (11) were obtained at each value of $\bar{\alpha}$. The real $\bar{p}$ solutions of equation (11) were used to find $\bar{q}$, $\bar{r}$, and $\bar{\beta}$ (eqs. (8), (9), and (10)). The resulting values were substituted into equation (5) and a residual was computed. If the residual from equation (5) changes signs between successive values of $\bar{\alpha}$, a common root of equations (5) and (11) exists. If the common root was not a root of the determinant (eq. (7)), a straight line fit was made between the $\bar{\alpha}$ values to find an approximation to the angle of attack which would yield a zero residual. This generally resulted in a residual from equation (5) of less than about $10^{-6}$ which was considered adequate for determining simultaneous solutions to equations (5) and (11). If the residual was greater than $10^{-6}$, a second straight line fit was made between the new value of $\bar{\alpha}$ and the value associated with the smaller of the original two residuals. This procedure was repeated until the residual was reduced to less than $10^{-6}$. It should be noted that, during the $\bar{\alpha}$ search, it was necessary to track multiple $\bar{p}$ solution branches to identify which $\bar{p}$ caused the sign change in the residual.

Having determined the values of $\bar{p}$, $\bar{\alpha}$, $\bar{q}$, $\bar{r}$, and $\bar{\beta}$ which satisfy equations (5) and (11), the linearized stability characteristics for perturbations about these PSS solutions were calculated. The $\bar{\alpha}$ search was then continued until all PSS solutions were obtained for the specified set of control inputs. This search procedure was implemented on both a high-speed computer and a minicomputer, and simultaneous solutions of equations (5) and (11) were obtained rapidly for any combination of control inputs.

25

## REFERENCES

1. Phillips, William H.: Effect of Steady Rolling on Longitudinal and Directional Stability. NACA TN 1627, 1948.

2. Pinsker, W. J. G.: Charts of Peak Amplitudes in Incidence and Sideslip in Rolling Manoeuvres Due to Inertia Cross Coupling. R. & M. No. 3293, British A.R.C., 1962.

3. Rhoads, Donald W.; and Schuler, John M.: A Theoretical and Experimental Study of Airplane Dynamics in Large Disturbance Maneuvers. J. Aeronaut. Sci., vol. 24, no. 7, July 1957, pp. 507-526, 532.

4. Walsh, G. R.: Forced Autorotation in the Rolling Motion of an Aeroplane. Aeronaut. Q., vol. XVII, pt. 3, Aug. 1966, pp. 269-283.

5. Sternfield, Leonard: A Simplified Method for Approximating the Transient Motion in Angles of Attack and Sideslip During A Constant Rolling Maneuver. NACA Rep. 1344, 1958. (Supersedes NACA RM L56F04.)

6. Hacker, T.; and Oprisiu, C.: A Discussion of the Roll-Coupling Problem. Progress in Aerospace Sciences, Volume 15, D. Küchemann, P. Carrière, B. Etkin, W. Fiszdon, N. Rott, J. Smolderen, I. Tani, and W. Wuest, eds., Pergamon Press, c.1974, pp. 151-180.

7. Schy, A. A.; and Hannah, M. E.: Prediction of Jump Phenomena in Roll-Coupled Maneuvers of Airplanes. J. Aircr., vol. 14, no. 4, Apr. 1977, pp. 375-382.

8. Young, J. W.; Schy, A. A.; and Johnson, K. G.: Prediction of Jump Phenomena in Aircraft Maneuvers, Including Nonlinear Aerodynamic Effects. J. Guid. & Control, vol. 1, no. 1, Jan.-Feb. 1978, pp. 26-31.

9. Mehra, Raman K.; Kessel, William C.; and Carroll, James V.: Global Stability and Control Analysis of Aircraft At High Angles-of-Attack. ONR-CR-215-248-1, U.S. Navy, June 1977. (Available from DTIC as AD A051 850.)

10. Mehra, Raman K.; and Carroll, James V.: Global Stability and Control Analysis of Aircraft At High Angles-of-Attack. Rep. ONR-CR 215-248-3, Aug. 1979.

11. Adams, William M., Jr.: Analytic Prediction of Airplane Equilibrium Spin Characteristics. NASA TN D-6926, 1972.

12. Adams, William M., Jr.: SPINEQ: A Program for Determining Aircraft Equilibrium Spin Characteristics Including Stability. NASA TM-78759, 1978.

13. Anglin, Ernie L.: Static Force Tests of a Model of a Twin-Jet Fighter Airplane for Angles of Attack From $-10^{\circ}$ to $110^{\circ}$ and Sideslip Angles From $-40^{\circ}$ to $40^{\circ}$. NASA TN D-6425, 1971.

14. Grafton, Sue B.; and Libbey, Charles E.: Dynamic Stability Derivatives of a Twin-Jet Fighter Model for Angles of Attack From $-10^{\circ}$ to $110^{\circ}$. NASA TN D-6091, 1971.

15. Chambers, Joseph R.; Bowman, James S., Jr.; and Anglin, Ernie L.: Analysis of the Flat-Spin Characteristics of a Twin-Jet Swept-Wing Fighter Airplane. NASA TN D-5409, 1969.

TABLE I.- WEIGHT, INERTIA, AND DIMENSIONAL CHARACTERISTICS OF AIRCRAFT

Weight, W, N . . . . . . . . . . . . . . . . . . . . . . . . . . . . . . . . . . . . . . 160 968

Moments of inertia, kg-m$^2$:
  $I_X$ . . . . . . . . . . . . . . . . . . . . . . . . . . . . . . . . . . . . . . . . . . . 35 398
  $I_Y$ . . . . . . . . . . . . . . . . . . . . . . . . . . . . . . . . . . . . . . . . . . 157 576
  $I_Z$ . . . . . . . . . . . . . . . . . . . . . . . . . . . . . . . . . . . . . . . . . . 178 460
  $I_{XZ}$ . . . . . . . . . . . . . . . . . . . . . . . . . . . . . . . . . . . . . . . . . 0

Wing area, S, m$^2$ . . . . . . . . . . . . . . . . . . . . . . . . . . . . . . . . . . . 49.2

Wing span, b, m . . . . . . . . . . . . . . . . . . . . . . . . . . . . . . . . . . . . 11.7

Mean aerodynamic chord, $\bar{c}$, m . . . . . . . . . . . . . . . . . . . . . . . . . . . . . 4.9

## TABLE II.- AERODYNAMIC DATA

[Control derivative units are per degree; all others are per radian]

| $\alpha$, deg | $c_X$ | $c_{X_{\delta_e}}$ | $c_Z$ | $c_{Z_{\delta_e}}$ | $c_{n_\beta}$ | $c_{n_p}$ | $c_{n_r}$ | $c_{n_{\delta_a}}$ | $c_{n_{\delta_r}}$ | $c_{m_q}$ | $c_m$ |
|---|---|---|---|---|---|---|---|---|---|---|---|
| -10 | -0.0334 | 0.00109 | 0.721 | -0.00650 | 0.1200 | 0.0289 | -0.35 | 0.00004 | -0.00091 | -2.7 | 0.0800 |
| -5 | -.0469 | .00119 | .360 | -.00650 | .1200 | .0081 | -.35 | .00004 | -.00088 | -2.7 | .0400 |
| 0 | -.0477 | .00102 | -.010 | -.00650 | .1200 | .0015 | -.35 | .00004 | -.00090 | -2.7 | .0100 |
| 5 | -.0320 | .00118 | -.384 | -.00652 | .1200 | .0004 | -.35 | .00004 | -.00081 | -2.7 | -.0200 |
| 10 | -.0173 | .00114 | -.673 | -.00681 | .0970 | .0085 | -.35 | .00007 | -.00068 | -2.7 | -.0380 |
| 15 | -.0177 | .00120 | -.895 | -.00681 | .0745 | .0186 | -.40 | .00015 | -.00064 | -4.0 | -.0590 |
| 20 | -.0442 | .00071 | -1.004 | -.00543 | .0344 | -.0756 | -.60 | .00027 | -.00061 | -5.4 | -.0810 |
| 25 | -.0527 | .00027 | -1.051 | -.00576 | -.1375 | .0079 | -.65 | .00019 | -.00057 | -5.2 | -.1000 |
| 30 | -.0414 | .00009 | -1.195 | -.00514 | -.2177 | .1378 | -.45 | .00019 | -.00044 | -4.5 | -.1330 |
| 35 | -.0430 | -.00058 | -1.313 | -.00786 | -.2349 | .0506 | -.20 | .00016 | -.00035 | -4.5 | -.1950 |
| 40 | -.0421 | -.00085 | -1.375 | -.00763 | -.1490 | 0 | -.10 | .00011 | -.00011 | -5.5 | -.2274 |
| 45 | -.0329 | -.00092 | -1.416 | -.00529 | -.1014 | .0300 | -.05 | .00025 | -.00018 | -6.0 | -.2430 |
| 50 | -.0173 | -.00113 | -1.467 | -.00500 | -.0556 | .0600 | -.04 | .00020 | .00006 | -6.0 | -.2646 |
| 55 | -.0024 | -.00140 | -1.525 | -.00614 | -.0539 | .0596 | -.06 | .00016 | .00001 | -6.0 | -.2871 |
| 60 | .0158 | -.00137 | -1.599 | -.00762 | -.0894 | .0546 | 0 | .00017 | .00001 | -5.5 | -.3129 |
| 65 | .0170 | -.00201 | -1.558 | -.00346 | -.1209 | .1151 | .06 | .00007 | .00024 | -3.5 | -.3883 |
| 70 | .0156 | -.00224 | -1.556 | -.00205 | -.1031 | .2147 | .10 | -.00008 | .00010 | -2.0 | -.4304 |
| 75 | .0165 | -.00229 | -1.573 | -.00224 | -.1226 | .5374 | -.30 | .00013 | -.00009 | -2.5 | -.4783 |
| 80 | .0201 | -.00240 | -1.562 | -.00157 | -.2229 | .9108 | -.35 | .00024 | -.00010 | -3.3 | -.5053 |
| 85 | .0254 | -.00249 | -1.557 | -.00133 | -.3747 | .7463 | 0 | .00024 | -.00023 | -3.2 | -.5293 |
| 90 | .0227 | -.00261 | -1.566 | -.00224 | -.4500 | .6130 | .32 | .00024 | -.00011 | -2.6 | -.5710 |

29

TABLE II.- Concluded

| α, deg | $c_{m_{\delta_e}}$ (a) | | $c_{l_\beta}$ | $c_{l_p}$ | $c_{l_r}$ | $c_{l_{\delta_a}}$ | $c_{l_{\delta_r}}$ | $c_{Y_\beta}$ | $c_{Y_r}$ | $c_{Y_p}$ | $c_{Y_{\delta_a}}$ | $c_{Y_{\delta_r}}$ |
|---|---|---|---|---|---|---|---|---|---|---|---|---|
| -10 | -0.0070 | | -0.0500 | -0.3010 | -0.06 | -0.00070 | 0.00018 | -0.6300 | 0.72 | 0.0366 | 0.00009 | 0.00166 |
| -5 | -.0070 | | -.0500 | -.3010 | 0 | -.00070 | .00015 | -.6300 | .80 | .0366 | .00009 | .00153 |
| 0 | -.0070 | | -.0500 | -.3010 | .03 | -.00070 | .00022 | -.6300 | .82 | .0366 | .00009 | .00159 |
| 5 | -.0070 | | -.0917 | -.3014 | .07 | -.00070 | .00020 | -.6300 | .86 | .0366 | .00009 | .00145 |
| 10 | -.0081 | | -.1375 | -.2574 | .15 | -.00064 | .00017 | -.5730 | .84 | .0613 | .00009 | .00116 |
| 15 | -.0088 | | -.1260 | -.1022 | .25 | -.00050 | .00011 | -.5730 | .75 | .1097 | -.00022 | .00124 |
| 20 | -.0072 | | -.0570 | -.0991 | .50 | -.00046 | .00006 | -.5160 | .50 | .2894 | -.00032 | .00106 |
| 25 | -.0060 | | 0 | -.2720 | .62 | -.00027 | .00003 | -.3720 | 0 | .3630 | -.00019 | .00132 |
| 30 | -.0055 | | .0230 | -.3060 | .48 | -.00020 | .00004 | -.3000 | -.66 | .3158 | -.00015 | .00097 |
| 35 | -0.0055 | -0.00670 | 0 | -.2526 | .20 | -.00018 | .00002 | -.2900 | -.80 | .1612 | .00018 | .00064 |
| 40 | -.0043 | -.00580 | -.1146 | -.0092 | .07 | .00007 | 0 | -.2700 | -.30 | -.5118 | -.00032 | .00049 |
| 45 | -.0043 | -.00485 | -.1146 | -.0380 | .05 | -.00002 | .00007 | -.2600 | -.14 | -.7517 | -.00033 | .00026 |
| 50 | -.0036 | -.00368 | -.1141 | -.0690 | .03 | -.00006 | .00005 | -.2500 | -.34 | -.6646 | -.00028 | -.00006 |
| 55 | -.0029 | -.00209 | -.1398 | -.0921 | .01 | -.00001 | 0 | -.2400 | -.38 | -.6069 | 0 | -.00020 |
| 60 | 0 | -.00125 | -.1501 | -.0965 | 0 | 0 | .00003 | -.2200 | -.38 | -.5267 | -.00014 | .00001 |
| 65 | 0 | -.00311 | -.1455 | -.0805 | 0 | .00003 | .00002 | .0499 | -.38 | -.7643 | -.00022 | .00016 |
| 70 | 0 | -.00329 | -.1553 | -.1381 | .01 | .00007 | -.00001 | .1720 | -.27 | -1.0630 | -.00003 | .00019 |
| 75 | 0 | -.00408 | -.1719 | -.1991 | .02 | .00004 | .00002 | .1720 | -.60 | -.9094 | -.00010 | .00013 |
| 80 | 0 | -.00335 | -.1845 | -.1815 | .02 | -.00007 | 0 | -.0880 | -.90 | -.2661 | -.00016 | .00020 |
| 85 | 0 | -.00349 | -.1868 | -.2040 | .02 | -.00008 | .00009 | -.2740 | -.90 | -.6982 | -.00013 | .00014 |
| 90 | 0 | -.00350 | -.1900 | -.1990 | 0 | -.00005 | .00004 | -.3500 | -1.00 | -1.1560 | -.00010 | .00020 |

aFor α = 35° to 90°, the left column of values is for $\delta_e \gtreqless 0$, and the right column for $\delta_e < 0$.

## TABLE III.- TRIM CONDITIONS

| $\Delta\delta_e$, deg | $\alpha$, deg | Pitch rate, deg/sec | Normal acceleration, g units |
|---|---|---|---|
| 8 | -3.8 | -3.1 | -0.6 |
| 6 | -1.5 | -2.6 | -.2 |
| 4 | .74 | -1.7 | .2 |
| 2 | 3 | -.9 | .6 |
| 0 | 5.5 | 0 | 1 |
| -4 | 15.3 | 2.3 | 2.1 |
| -8 | 19.6 | 2.6 | 2.22 |
| -12 | 23.5 | 2.5 | 2.18 |

# TABLE IV.- STABILITY CHARACTERISTICS OF
## ONE-G TRIM SOLUTIONS

| Curve | $\delta_a$, deg | Characteristic roots | | |
|-------|-----------------|----------|----------|----------|
| 1P | 0 | -0.69 | -0.31 ± 1.50i | -0.24 ± 2.1i |
|    | -15 | -.62 | -.36 ± 1.40i | -.25 ± 2.7i |
|    | -30 | -.81 | -.25 ± 1.70i | -.11 ± 3.0i |
| 2N | 0 | 2.00 | -1.38 ± 0.56i | -.55 ± 2.9i |
|    | -15 | 1.60 | -.68 ± 1.60i | -.89 ± 3.0i |
|    | -30 | .53 | -.57 ± 1.60i | -.41 ± 3.2i |
| 2P | 0 | 2.00 | -1.38 ± 0.56i | -.55 ± 2.9i |
|    | -15 | 2.20 | -1.71 ± 0.48i | -.19 ± 3.6i |
|    | -25 | 2.30 | -1.78 ± 1.30i | -.13 ± 3.7i |
| 3P | 0 | -2.20 | 1.58 ± 2.50i | -1.00 ± 3.4i |
|    | -15 | -2.30 | 1.42 ± 2.20i | -.88 ± 3.2i |
|    | -25 | -2.70 | 1.33 ± 1.70i | -.69 ± 3.0i |
| 3N | 0 | -2.20 | 1.58 ± 2.50i | -1.00 ± 3.4i |
|    | -15 | -2.30 | 1.71 ± 2.70i | -1.10 ± 3.6i |
|    | -30 | -2.40 | 1.82 ± 2.80i | -1.10 ± 3.7i |
| 4N | 0 | .40 | -.91 ± 3.00i | .25 ± 3.6i |
|    | -15 | 1.10 | -1.30 ± 2.90i | .41 ± 3.5i |
|    | -30 | 1.40 | -1.50 ± 2.90i | .42 ± 3.6i |
| 4P | 0 | .40 | -.91 ± 0.30i | .25 ± 3.6i |
|    | -15 | .30 | -.54 ± 3.20i | -.10 ± 4.1i |
|    | -30 | 1.00 | -.72 ± 3.90i | -.17 ± 4.5i |
| 5N | 0 | -1.90 | -.33 ± 5.70i | .90 ± 3.5i |
|    | -15 | -1.80 | -.32 ± 5.70i | .83 ± 3.4i |
|    | -30 | -1.60 | -.32 ± 5.70i | .74 ± 3.3i |
| 5P | 0 | -1.90 | -.33 ± 5.70i | .90 ± 3.5i |
|    | -15 | -2.10 | -.33 ± 5.70i | .97 ± 3.5i |
|    | -30 | -2.20 | -.33 ± 5.70i | 1.04 ± 3.6i |
| 6N | 0 | 2.80 | -.41 ± 7.70i | 1.43 ± 3.1i |
|    | -15 | 2.70 | -.40 ± 7.40i | 1.43 ± 3.1i |
|    | -30 | 2.70 | -.39 ± 7.30i | 1.44 ± 3.1i |
| 6P | 0 | 2.80 | -.41 ± 7.70i | 1.43 ± 3.1i |
|    | -15 | 2.80 | -.41 ± 8.00i | 1.43 ± 3.1i |
|    | -30 | 2.80 | -.42 ± 8.20i | 1.42 ± 3.1i |

TABLE V.- STABILITY CHARACTERISTICS OF BASIC AND ASSOCIATED SOLUTIONS

| $\Delta\delta_e$, deg | $\delta_a$, deg | Characteristic roots | | | |
|---|---|---|---|---|---|
| 8 | 0 | -0.92 | -0.130 ± 1.70i | | -0.36 ± 2.1i |
| | -4 | -.92 | -.190 ± 1.40i | | -.29 ± 2.4i |
| | -8 | -.94 | -.210 ± 1.00i | | -.27 ± 2.7i |
| | 0 | 0.63 | -1.100 ± 0.42i | | -0.10 ± 3.9i |
| | -4 | .57 | -1.000 ± .38i | | -.18 ± 3.9i |
| | -8 | .46 | -.960 ± .31i | | -.20 ± 3.7i |
| | 0 | -0.86 | -0.200 ± 1.60i | | -0.43 ± 3.9i |
| | -15 | -.97 | -.190 ± 1.30i | | -.36 ± 4.1i |
| | -30 | -.84 | -.310 ± 1.20i | | -.30 ± 4.1i |
| 6 | 0 | -0.90 | -0.150 ± 1.70i | | -0.36 ± 2.1i |
| | -5 | -.90 | -.220 ± 1.40i | | -.28 ± 2.5i |
| | -10 | -.90 | -.240 ± .80i | | -.24 ± 3.0i |
| | -5 | 0.54 | -0.21 | -1.80 | -2.40 ± 3.9i |
| | -10 | .20 | -.65 | -.97 | -2.10 ± 3.8i |
| | -5 | -1.40 | -0.100 ± 0.48i | | -0.27 ± 4.0i |
| | -15 | -.84 | -.340 ± .80i | | -.30 ± 4.1i |
| | -30 | -.82 | -.310 ± .97i | | -.28 ± 4.8i |
| 4 | 0 | -0.85 | -0.170 ± 1.80i | | -0.36 ± 2.1i |
| | -15 | -.65 | -.370 ± .60i | | -.27 ± 3.4i |
| | -25 | -.73 | -.320 ± .34i | | -.27 ± 3.8i |
| | -27 | -.85 | -.270 ± .02i | | -.24 ± 4.3i |
| | -30 | -.87 | -.270 ± .65i | | -.24 ± 4.7i |
| 2 | 0 | -0.78 | -0.200 ± 1.90i | | -0.36 ± 2.1i |
| | -15 | -.66 | -.370 ± 1.10i | | -.30 ± 3.2i |
| | -30 | -.95 | -.300 ± 1.10i | | -.18 ± 3.3i |
| 0 | 0 | -0.69 | -0.310 ± 1.50i | | -0.24 ± 2.1i |
| | -5 | -.63 | -.340 ± 1.30i | | -.23 ± 2.3i |
| | -15 | -.62 | -.360 ± 1.40i | | -.25 ± 2.7i |
| | -30 | -.81 | -.250 ± 1.70i | | -.11 ± 3.0i |
| -4 | 0 | -0.25 | -0.280 ± 2.20i | | -0.18 ± 2.5i |
| | -15 | -.45 | -.280 ± 2.10i | | -.14 ± 2.8i |
| | -30 | -.75 | -.200 ± 1.80i | | -.10 ± 3.2i |
| -8 | 0 | -0.35 | -0.170 ± 2.00i | | -0.36 ± 2.4i |
| | -15 | -.37 | -.320 ± 1.70i | | -.30 ± 2.8i |
| | -30 | -.42 | -.230 ± 1.30i | | -.28 ± 3.5i |
| -12 | 0 | -1.70 | 0.330 ± 0.52i | | -0.31 ± 2.3i |
| | -1 | -1.80 | .360 ± .41i | | -.32 ± 2.3i |
| | 0 | -2.50 | 1.6 | -0.22 | -0.43 ± 2.6i |
| | -1 | -2.30 | 1.4 | -.26 | -.35 ± 2.4i |

**TABLE VI.- COMPARISON OF PSS SOLUTIONS WITH EQUILIBRIUM SPIN CONDITIONS ($\Delta\delta_e = \delta_a = \delta_r = 0°$)**

| Method | $\alpha$, deg | $p$, deg/sec | $q$, deg/sec | $r$, deg/sec | $\beta$, deg | $V$, m/sec | Characteristic roots | | | | |
|---|---|---|---|---|---|---|---|---|---|---|---|
| Reference 11 | 35.7 | 75.9 | 2.50 | 54.6 | -0.90 | 187 | -2.00 | -0.10 | -0.05 ± 1.6i | 1.40 ± 2.0i | -0.80 ± 2.5i |
| PSS | 37.5 | 107.9 | .51 | 82.6 | -1.20 | 266 | -2.20 | | | 1.60 ± 2.5i | -1.00 ± 3.4i |
| PSS(D = W) | 37.6 | 73.3 | -.71 | 56.3 | -.86 | 181 | -1.50 | | | 1.20 ± 1.7i | -.80 ± 2.1i |
| PSS(D = W, γ = -90°) | 37.4 | 73.9 | 1.30 | 56.4 | -1.60 | 181 | -1.70 | | | 1.30 ± 1.7i | -.80 ± 2.1i |
| Reference 11 | 60.4 | 49.3 | 3.40 | 86.5 | 0.50 | 142 | -0.13 | 0.04 | -0.07 ± 1.7i | 0.20 ± 2.6i | -0.40 ± 2.4i |
| PSS | 49.3 | 100.2 | 1.30 | 116.3 | .40 | 266 | .40 | | | .30 ± 3.6i | -.90 ± 3.0i |
| PSS(D = W) | 46.6 | 62.1 | -.30 | 65.4 | 0 | 162 | .39 | | | .30 ± 2.0i | -.70 ± 1.6i |
| PSS(D = W, γ = -90°) | 52.2 | 56.7 | 1.10 | 72.8 | -1.00 | 153 | .18 | | | .04 ± 2.1i | -.40 ± 1.5i |
| Reference 11 | 73.1 | 40.9 | 1.60 | 133.5 | 0.10 | 136 | -0.42 | 0.15 | -0.07 ± 2.4i | 0.30 ± 2.9i | -0.20 ± 2.8i |
| PSS | 73.3 | 79.2 | -3.70 | 263.4 | -.90 | 266 | -1.90 | | | .90 ± 3.5i | -.30 ± 5.7i |
| PSS(D = W) | 73.6 | 40.2 | -3.80 | 135.5 | -.40 | 136 | -1.10 | | | .50 ± 1.6i | -.20 ± 2.9i |
| PSS(D = W, γ = -90°) | 73.3 | 40.6 | -1.20 | 134.4 | -1.00 | 136 | -1.10 | | | .50 ± 1.6i | -.20 ± 2.9i |
| Reference 11 | 82.1 | 28.9 | 1.50 | 206.0 | 0.23 | 134 | 0.27 | -0.15 | -0.06 ± 3.6i | -0.40 ± 3.4i | -0.01 ± 3.9i |
| PSS | 83.7 | 51.6 | -.80 | 460.7 | .03 | 266 | 2.80 | | | -1.40 ± 3.1i | -.40 ± 7.7i |
| PSS(D = W) | 83.9 | 25.5 | -1.60 | 235.3 | .50 | 133 | 1.40 | | | -.70 ± 1.5i | -.20 ± 3.9i |
| PSS(D = W, γ = -90°) | 83.7 | 26.1 | .01 | 230.4 | -.13 | 134 | 1.40 | | | -.70 ± 1.5i | -.20 ± 3.9i |
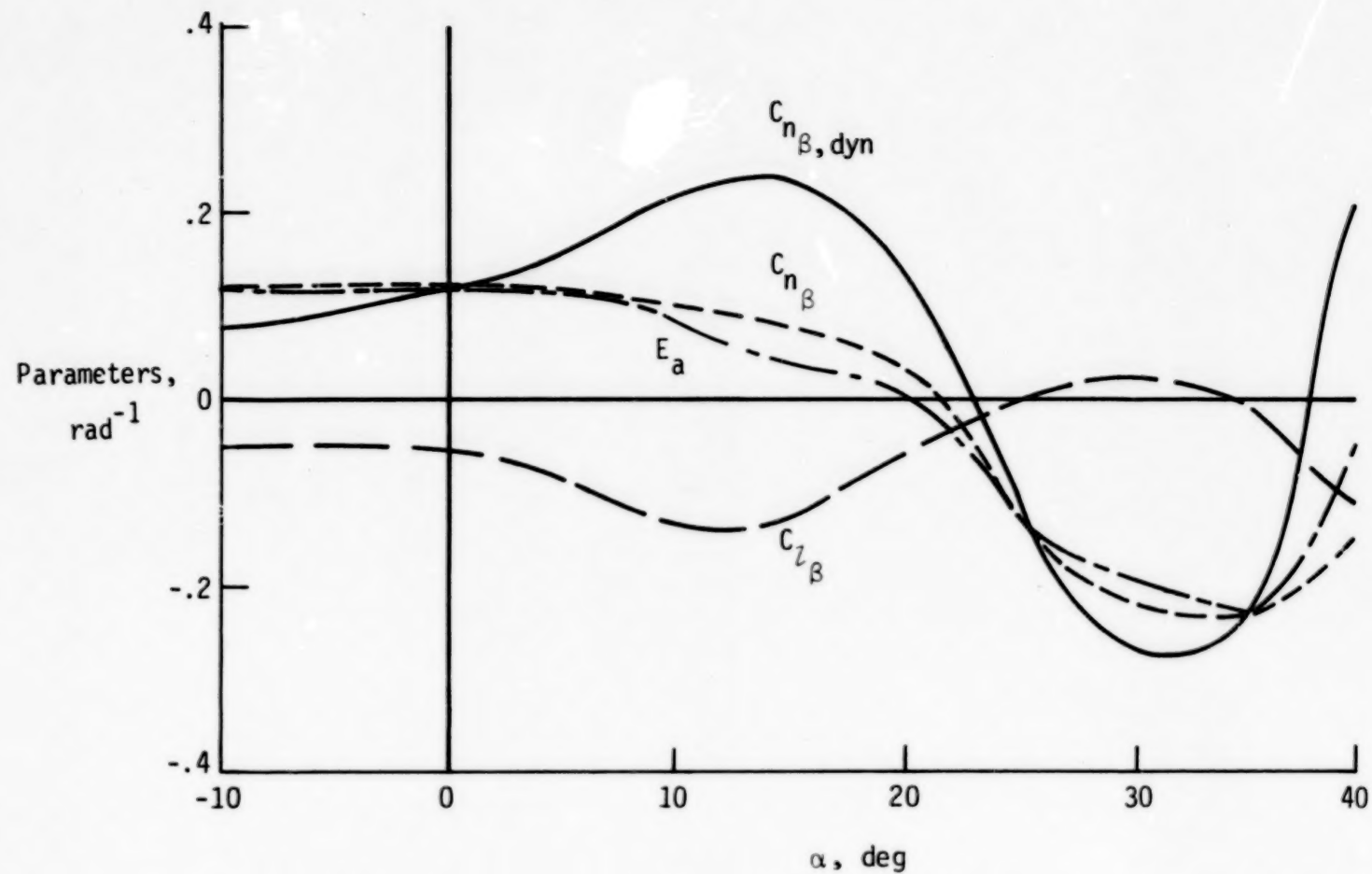
Figure 1.- Variation of lateral-directional stability and control characteristics with angle of attack.

BLANK PAGE

BLANK PAGE

P  Positive roll-rate solutions
N  Negative roll-rate solutions

Curves numbered 1 to 6 in order
of increasing angle of attack

——— Stable
—·—·— Unstable oscillation
——— Divergent
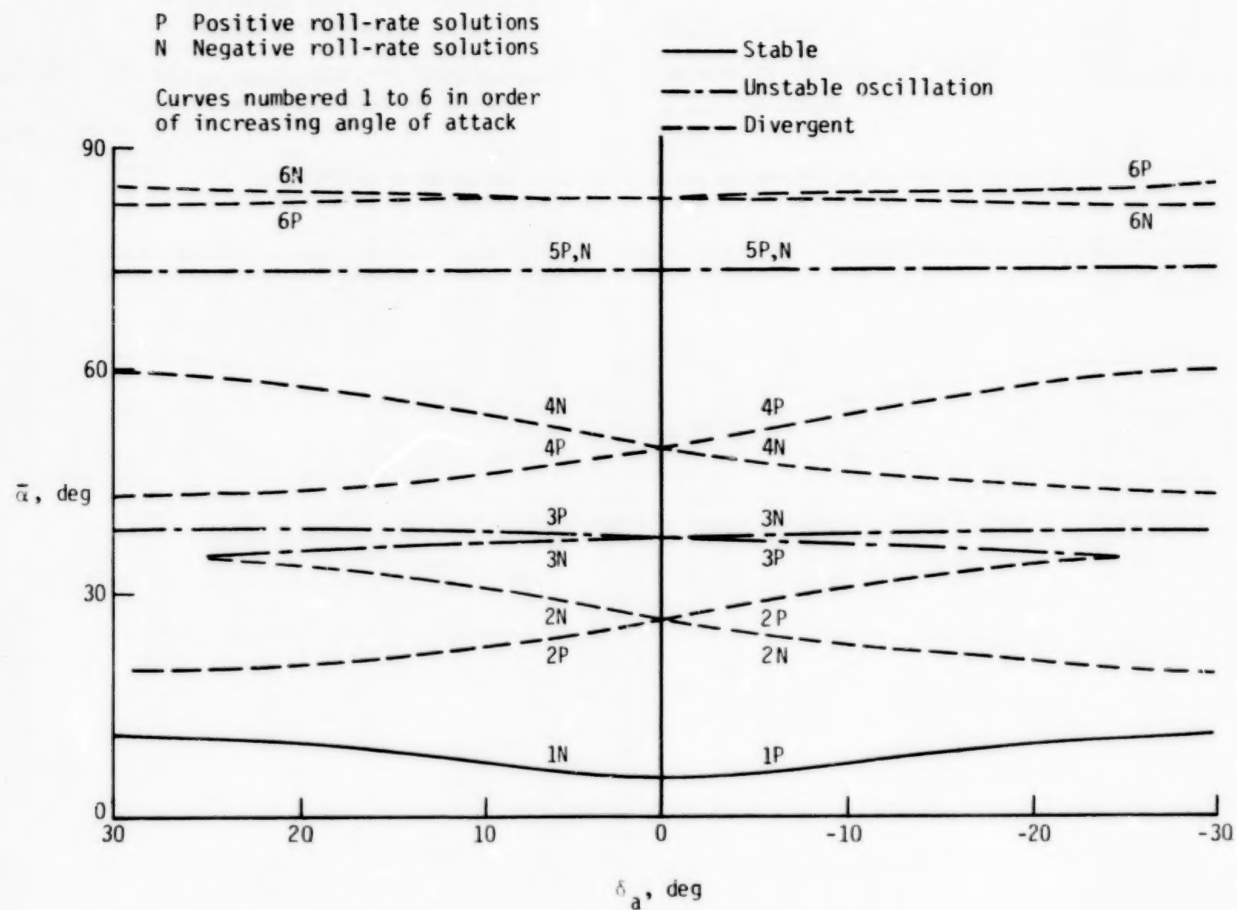
(a) Angle of attack.

Figure 2.- PSS solution for one-g trim condition $\Delta\delta_e = 0^o$.

36
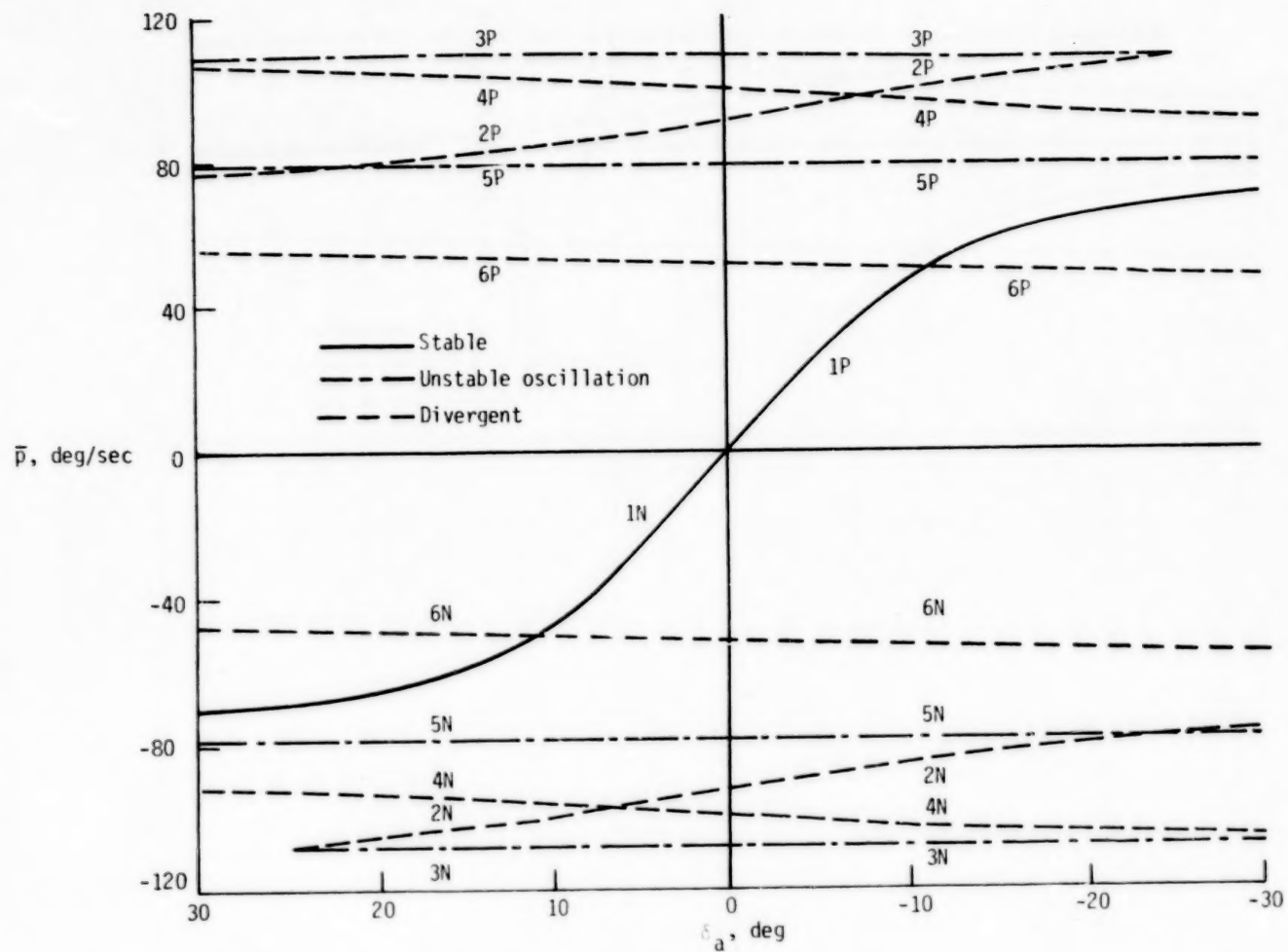
(b) Roll rate.

Figure 2.- Continued.

37
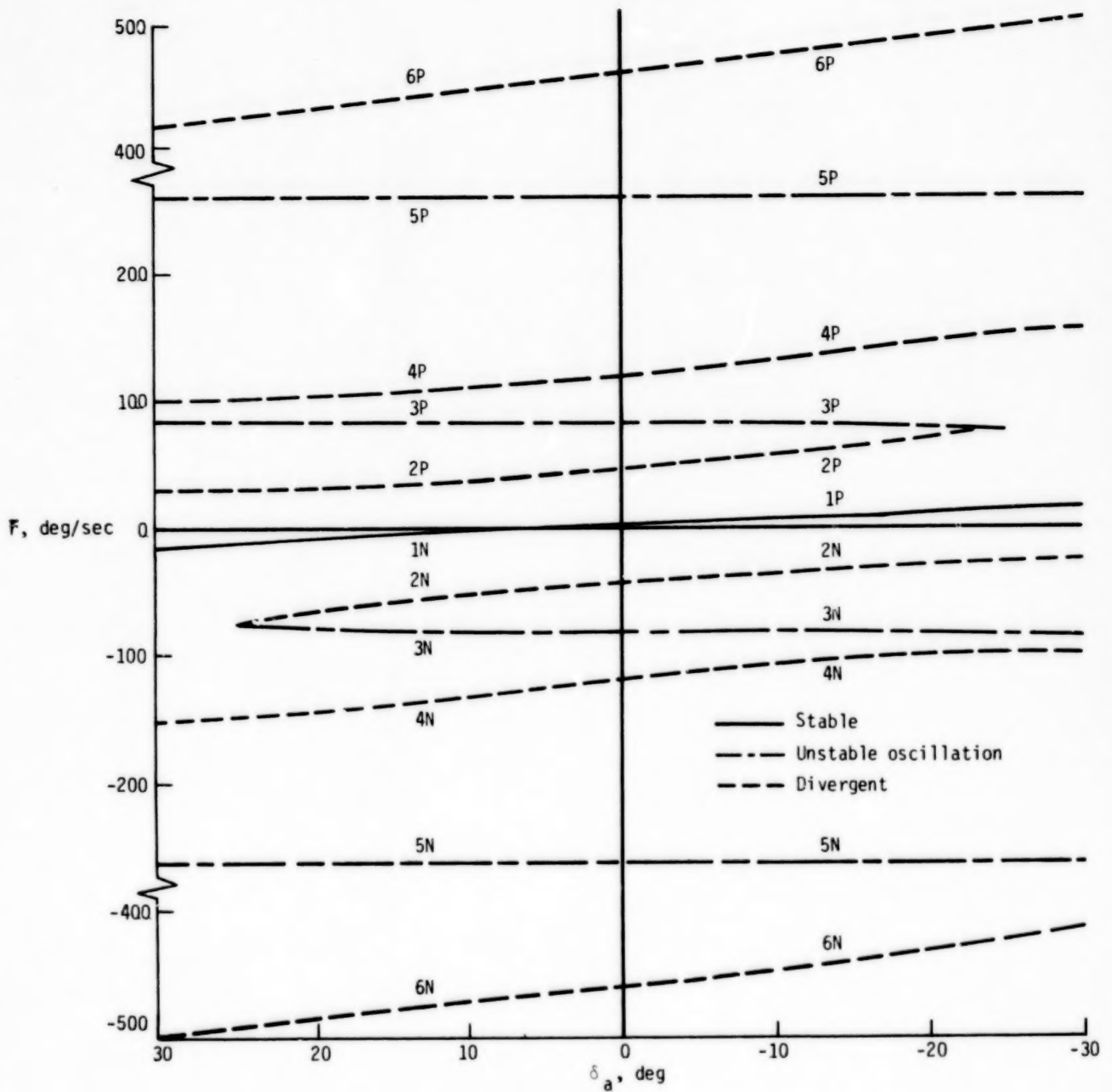
(c) Yaw rate.

Figure 2.- Continued.
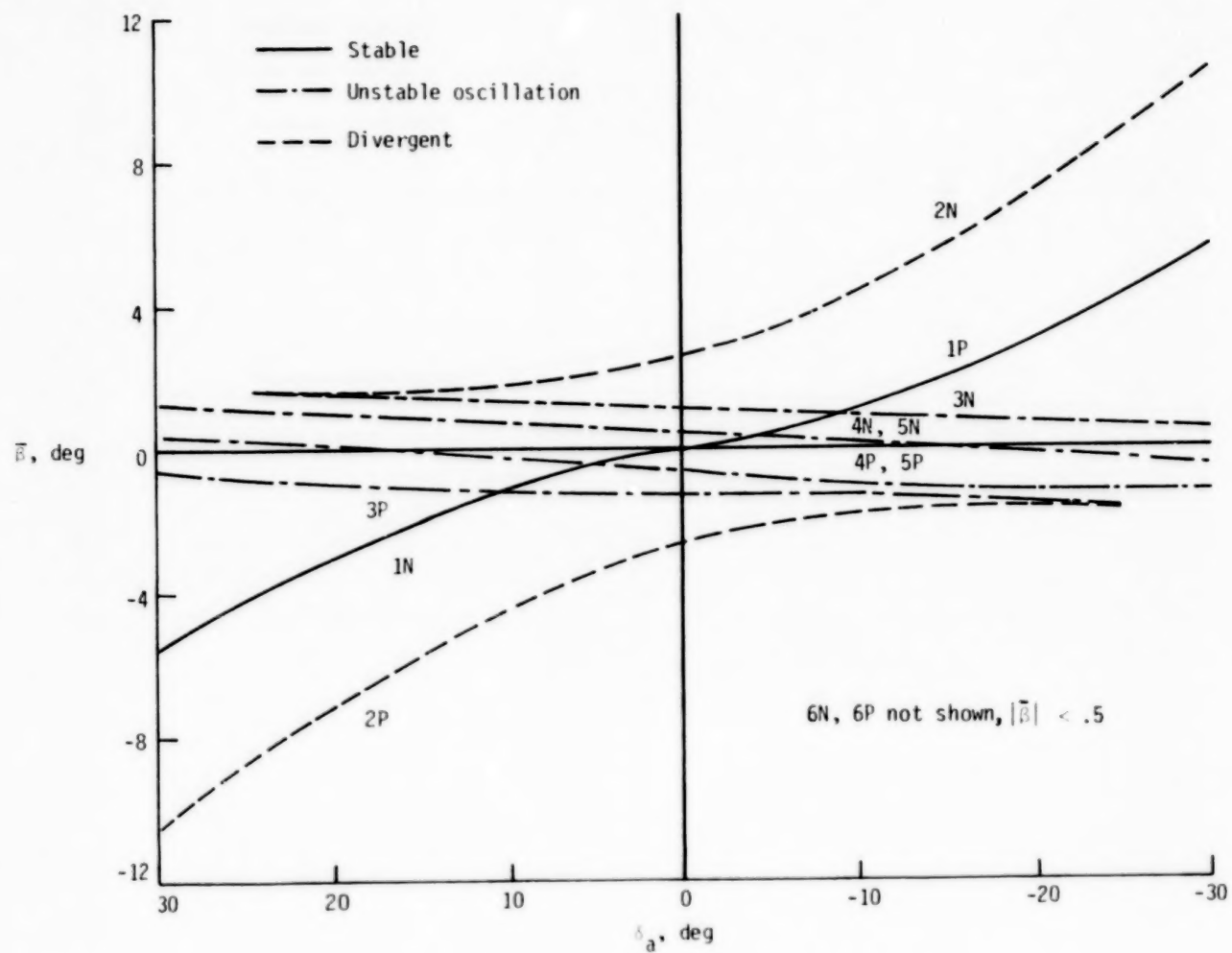
(d) Sideslip angle.

Figure 2.- Continued.
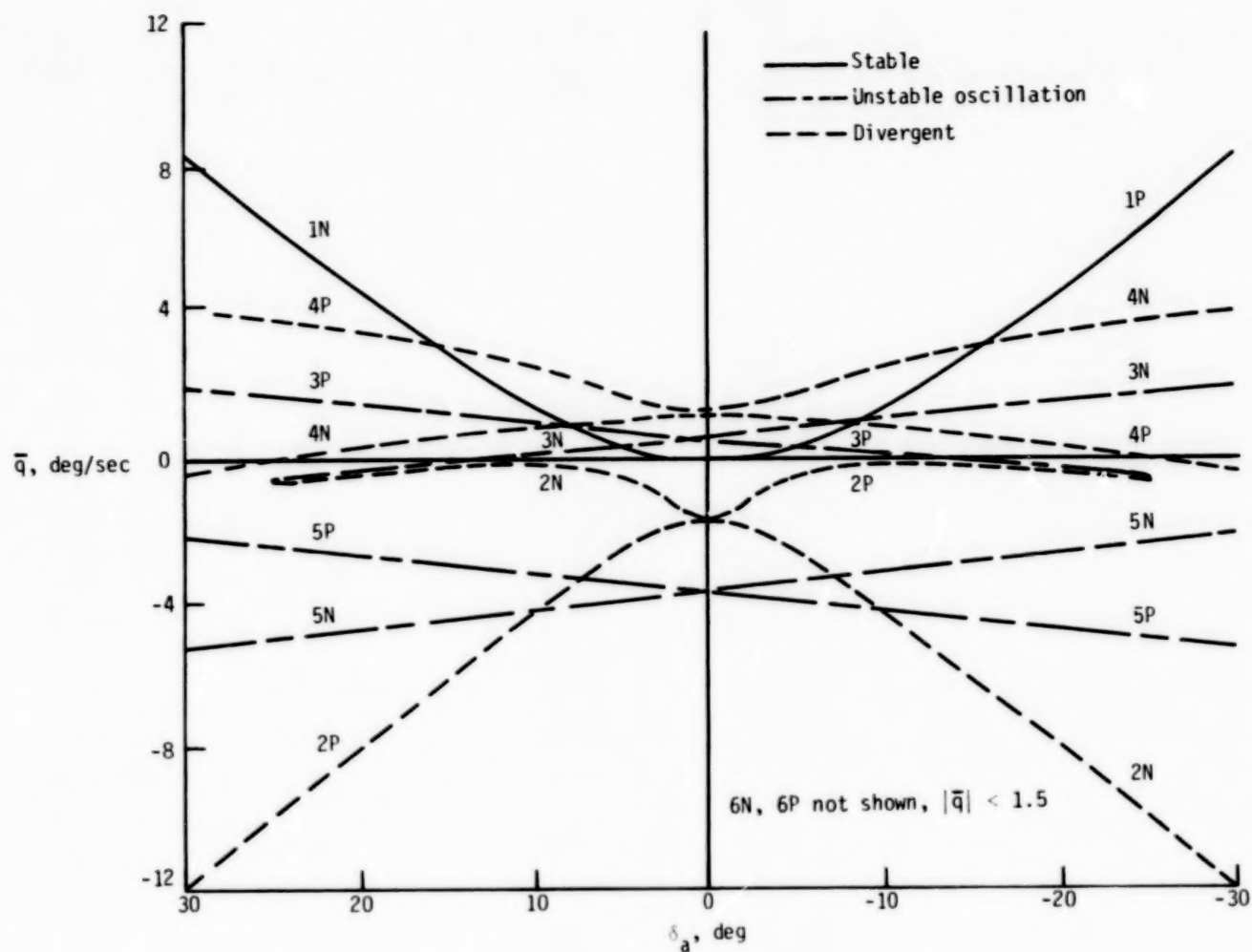
(e) Pitch rate.

Figure 2.- Concluded.
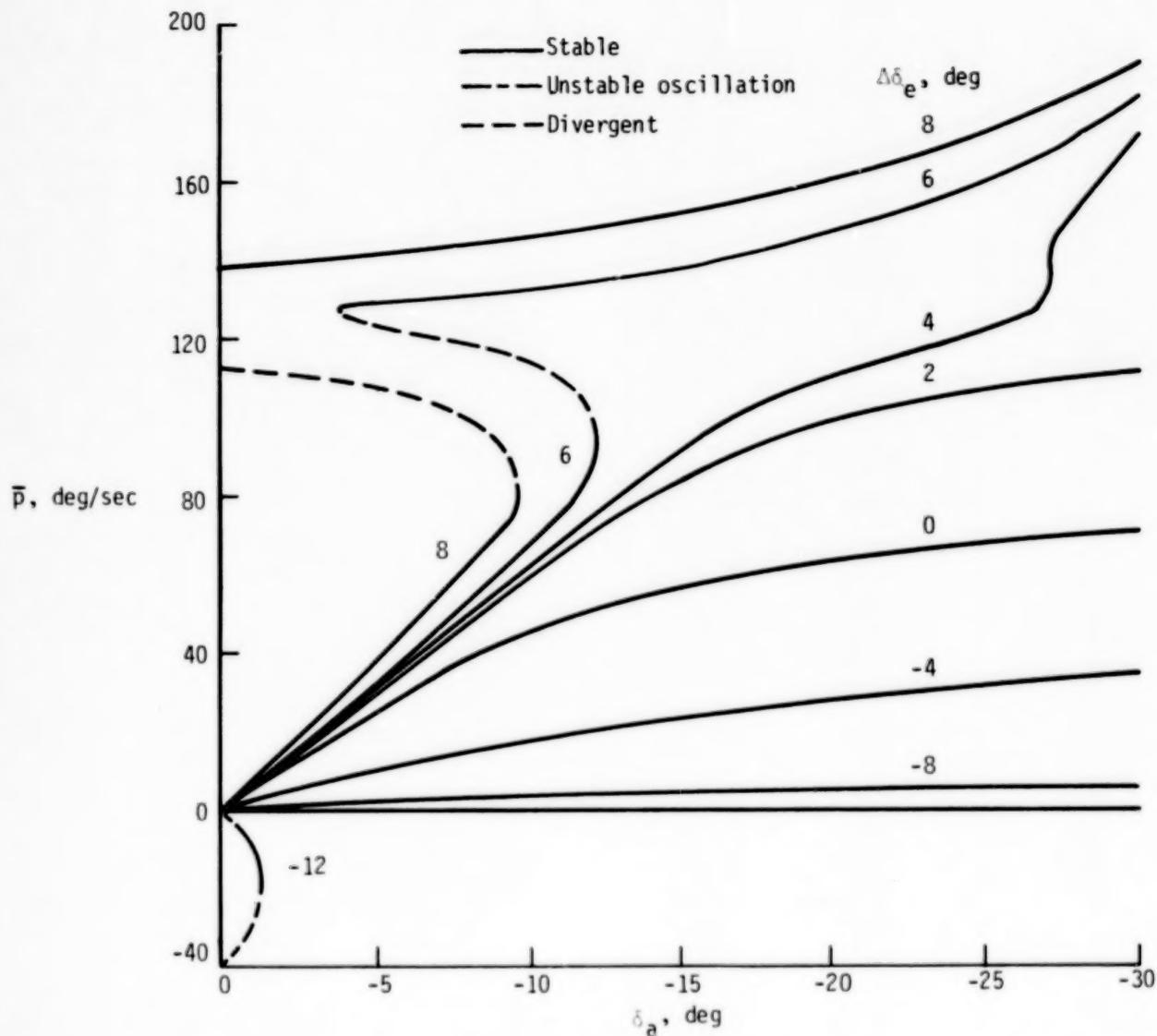
(a) Roll rate.

Figure 3.- Basic and associated PSS solutions with various elevator and aileron inputs for $\alpha < 25^\circ$.
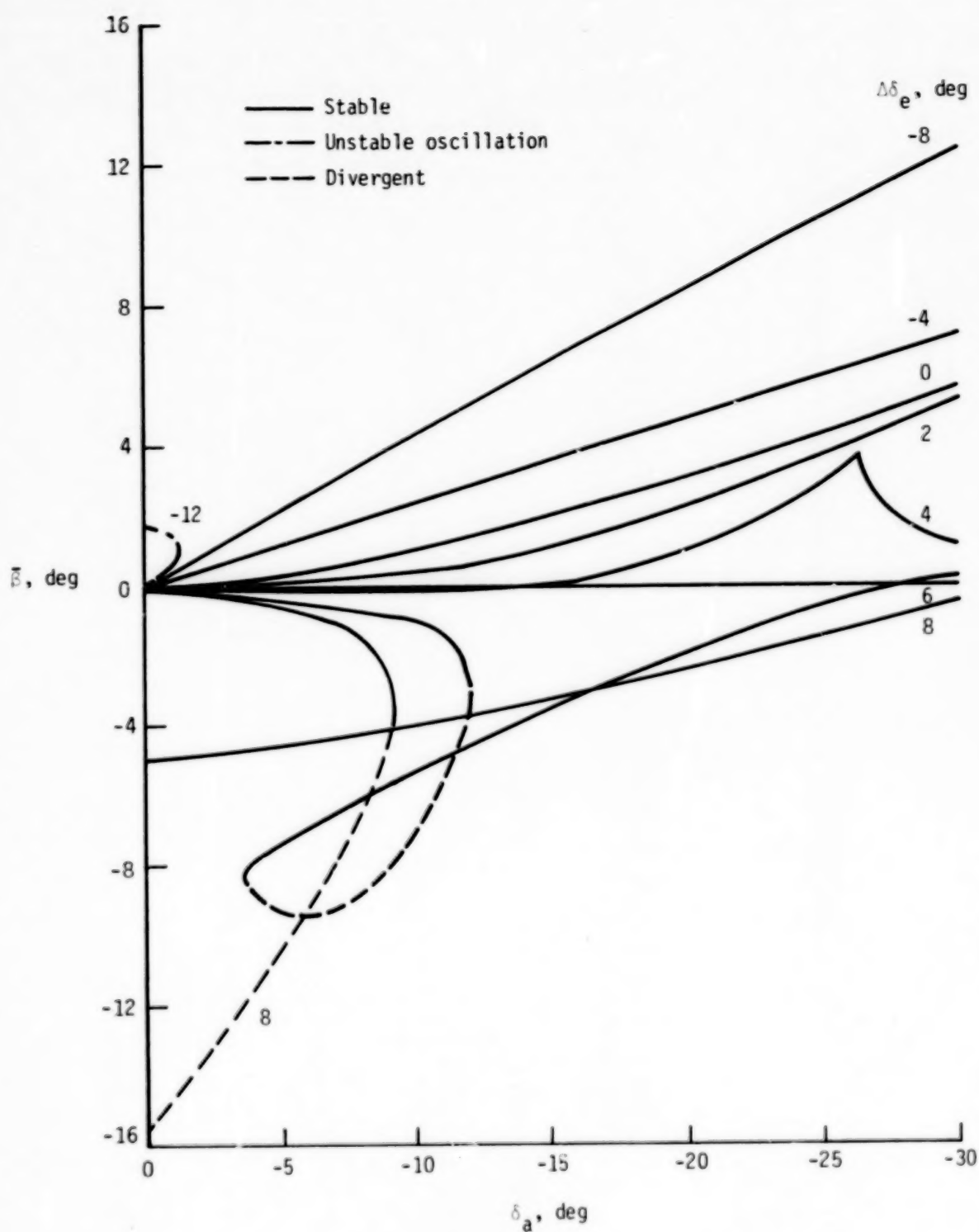
(b) Sideslip angle.

Figure 3.- Continued.
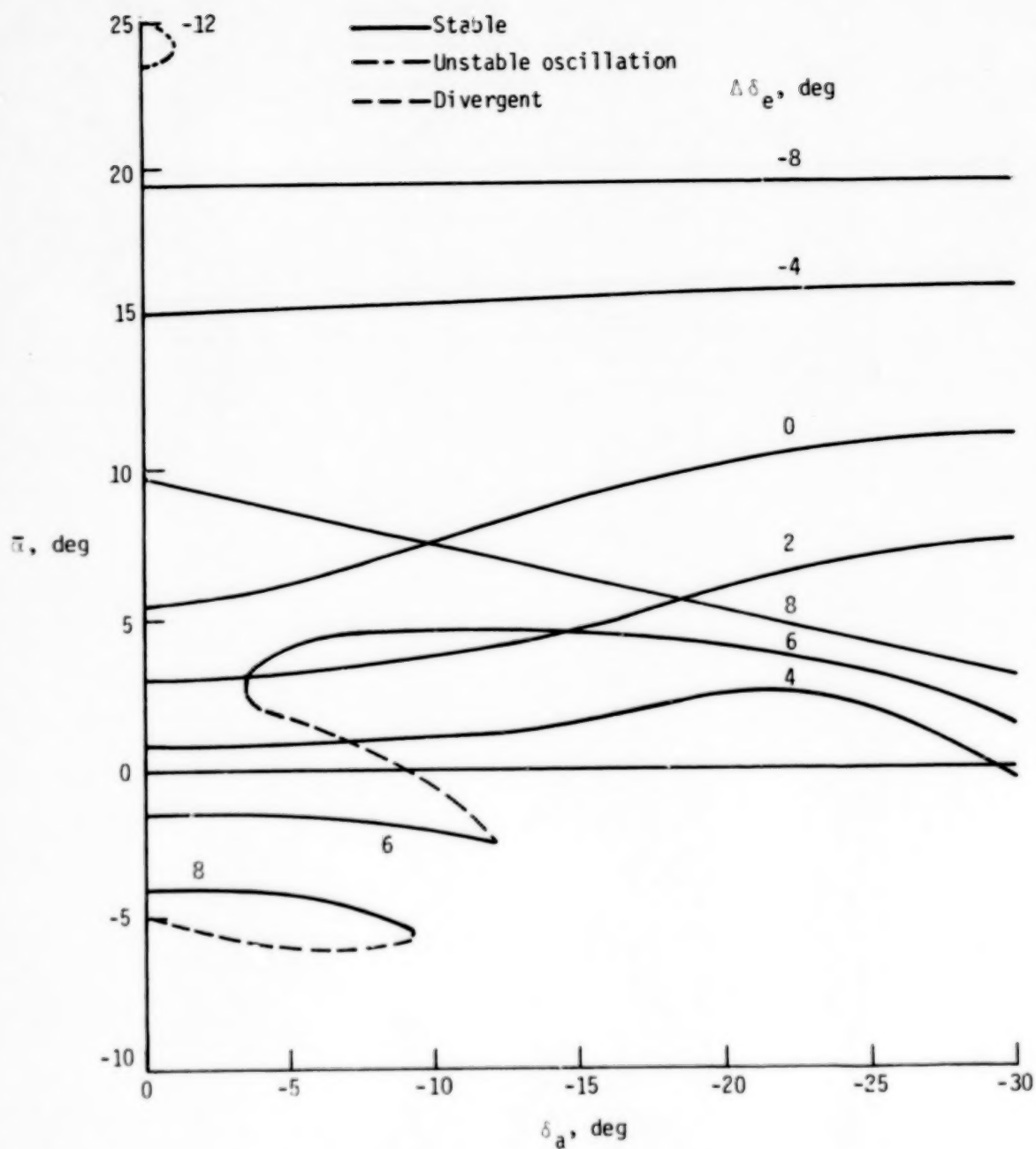
(c) Angle of attack.

Figure 3.- Continued.
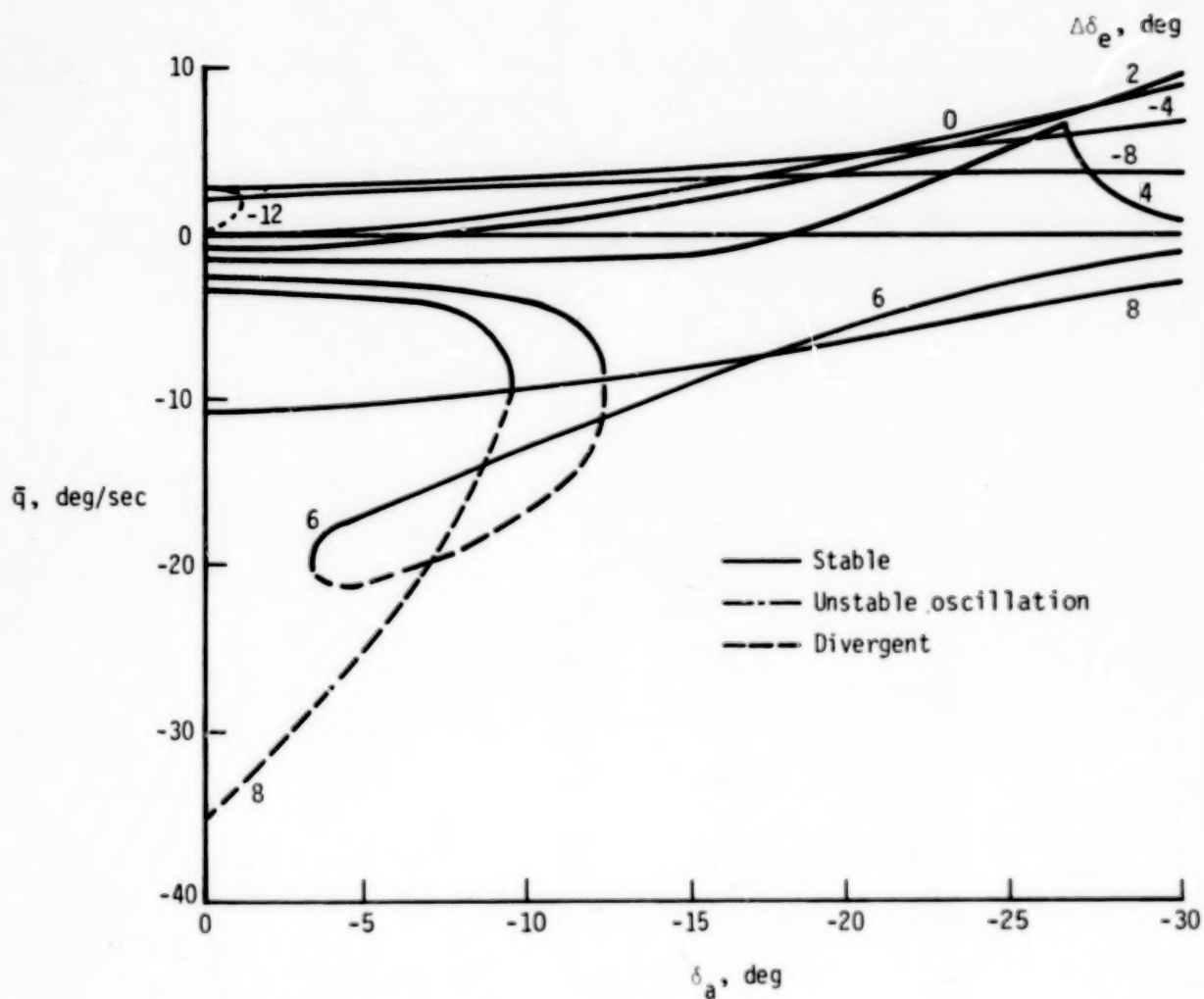
(d) Pitch rate.

Figure 3.- Continued.
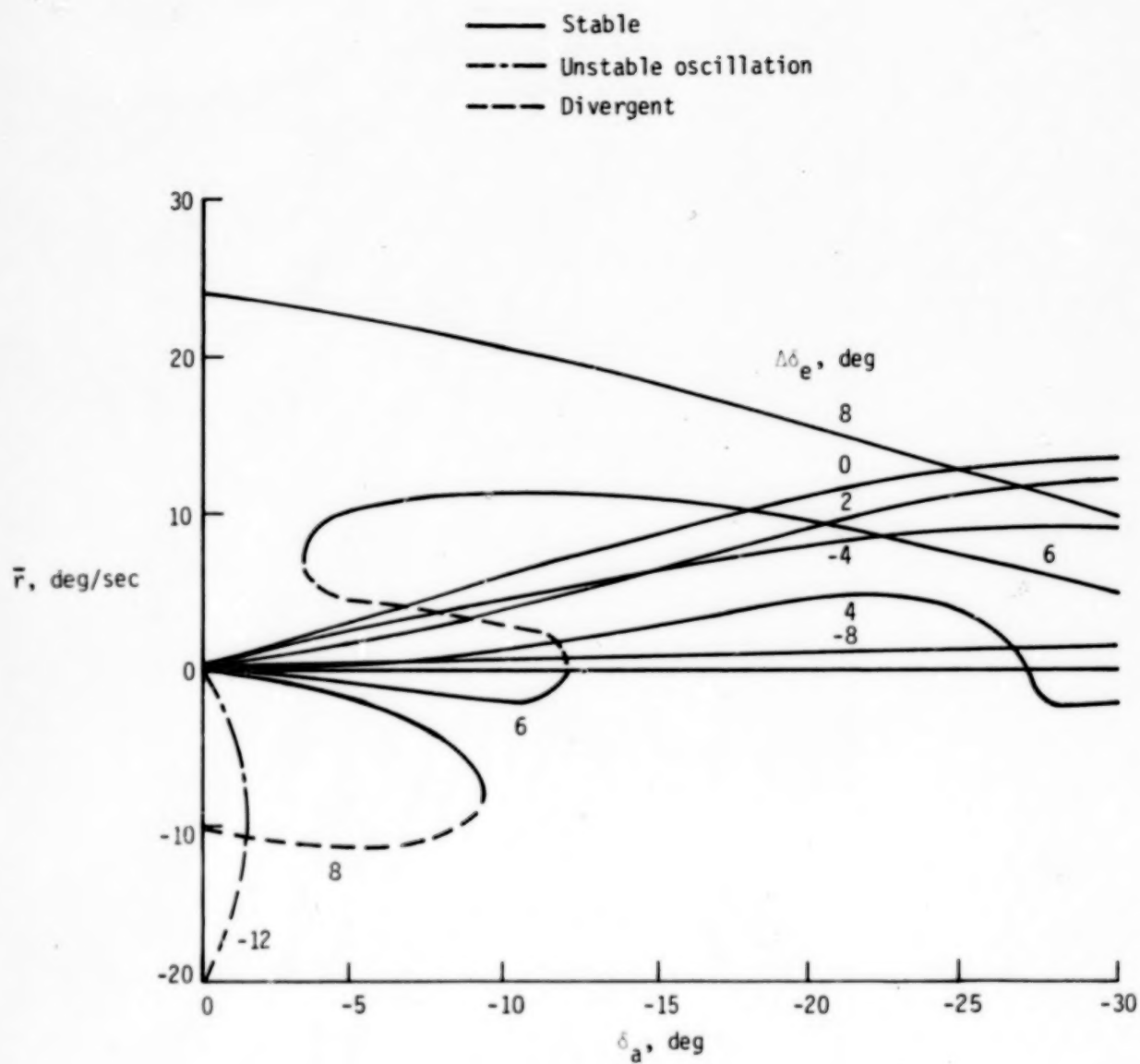
(e) Yaw rate.

Figure 3.- Concluded.
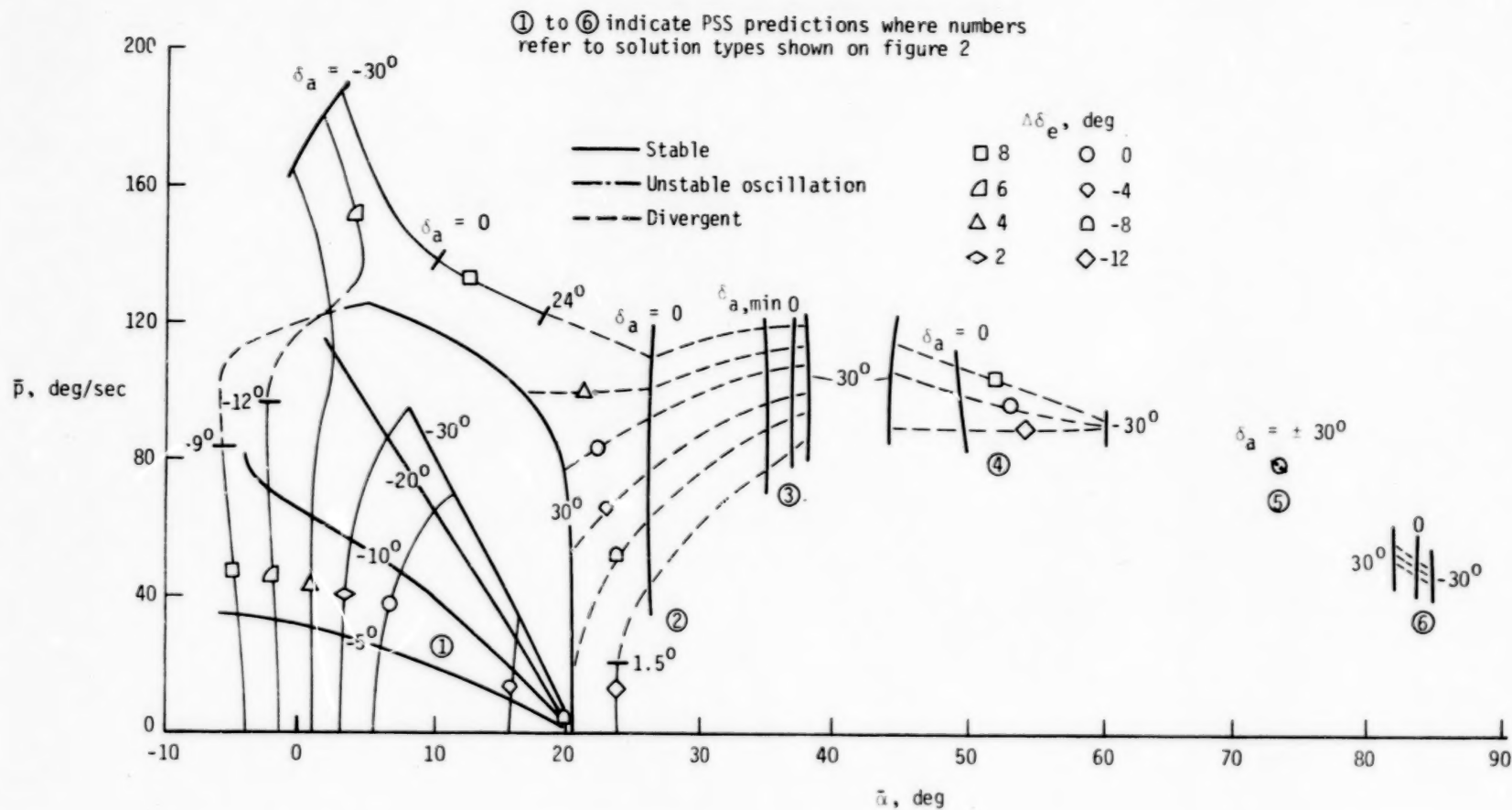
(a) Roll rate.

Figure 4.- Roll-rate and angular-velocity PSS solutions as a function of angle of attack. $\delta_{\bar{a},min}$ is the $\delta_a$ at which solutions 2 and 3 join (see fig. 2).

(b) Angular velocity.
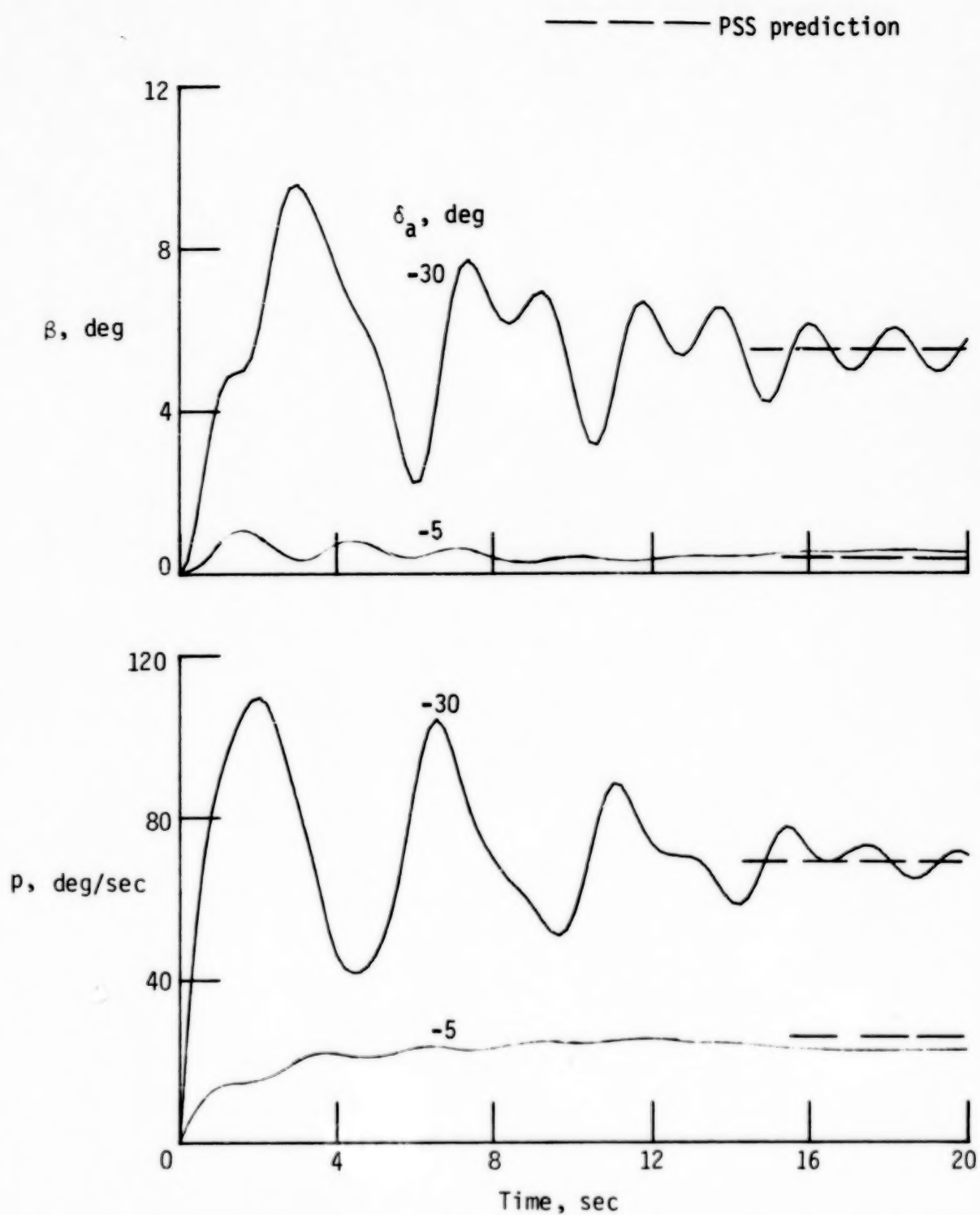
Figure 4.- Concluded.

Figure 5.- Calculated responses for two aileron inputs initiated from one-g trim condition. $\Delta\delta_e = 0°$; $\alpha = 5.5°$.
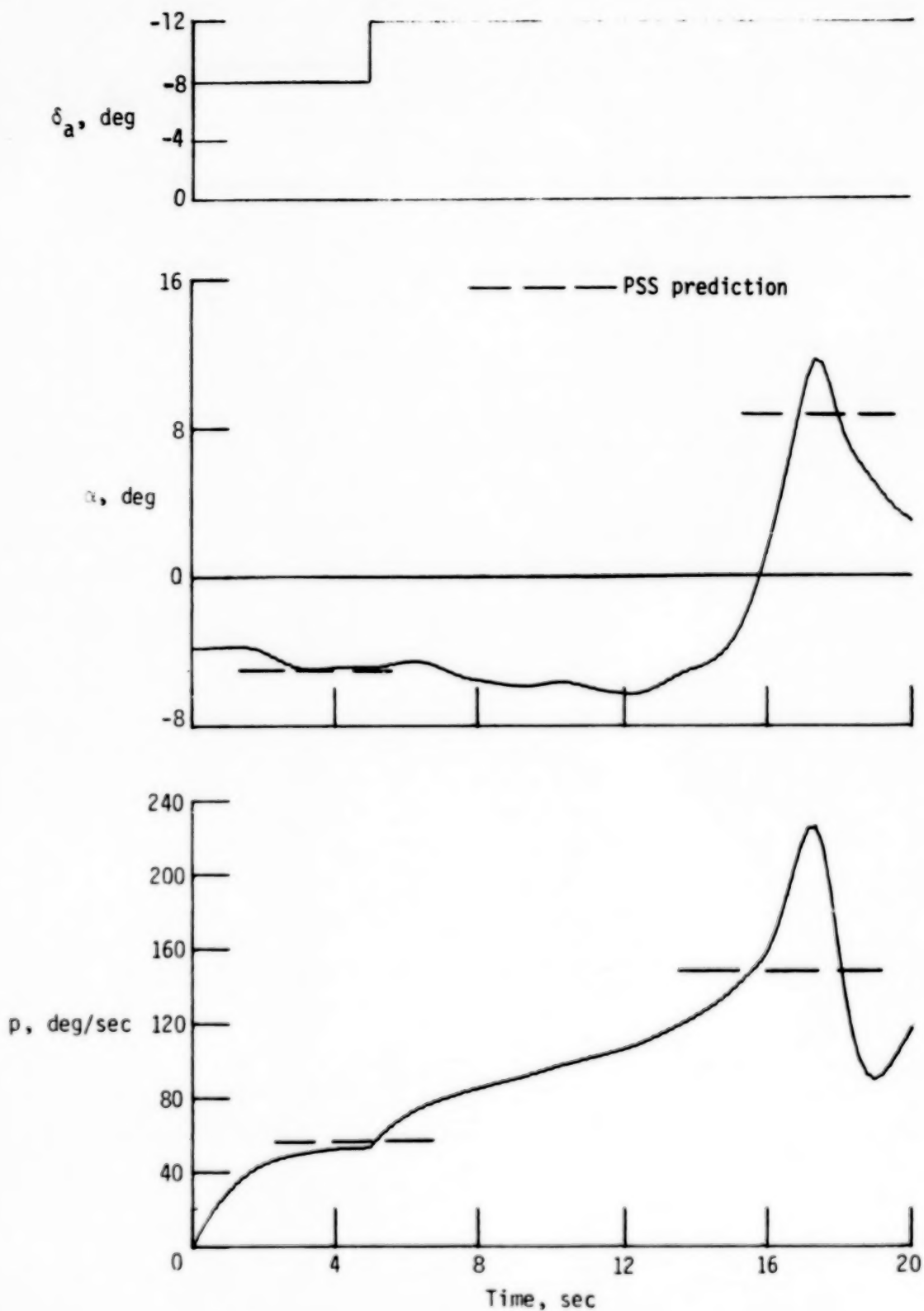
Figure 6.- Calculated responses initiated from pitch-down condition. $\Delta\delta_e = 8°$; $\alpha = -3.8°$.
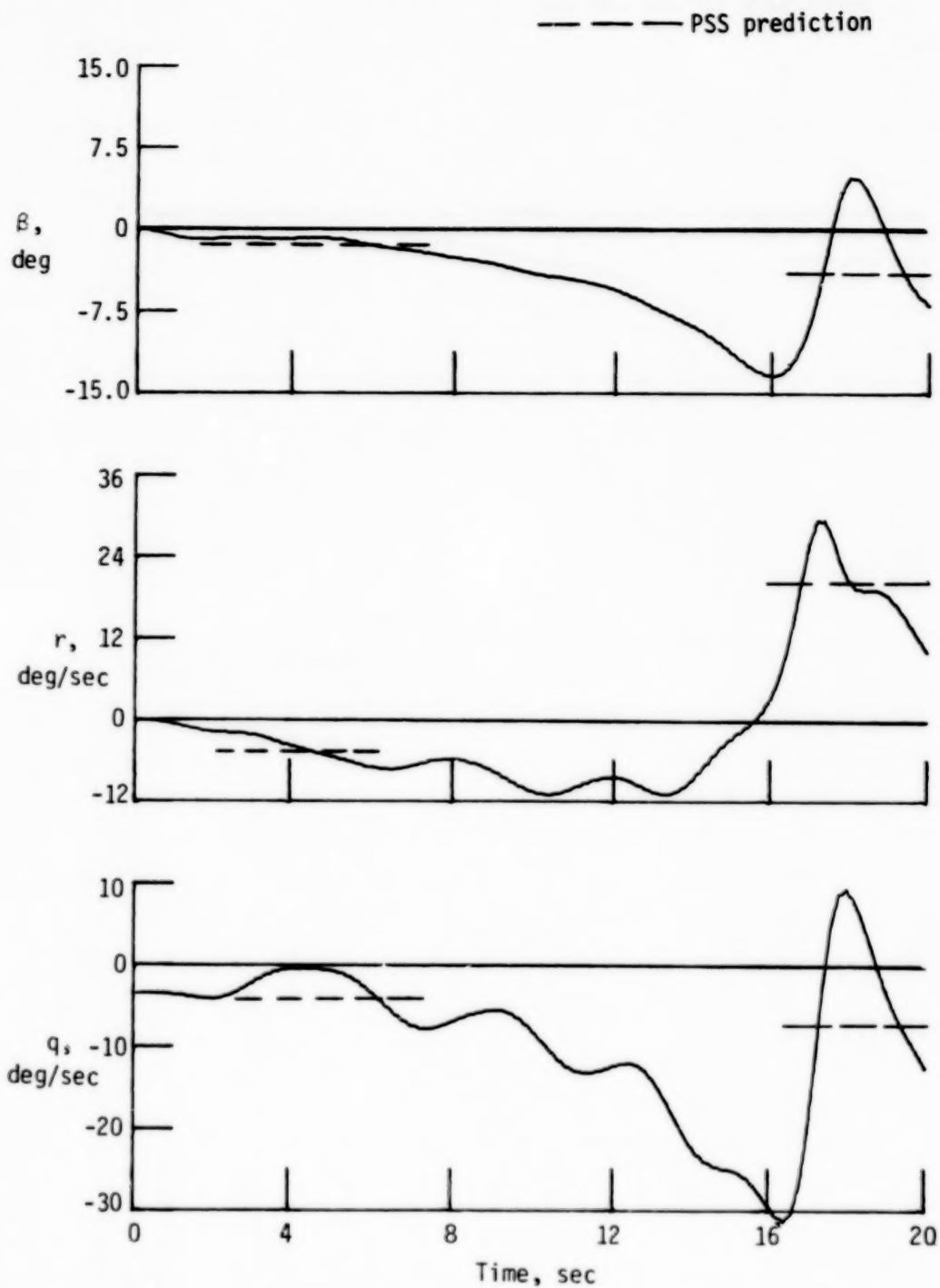
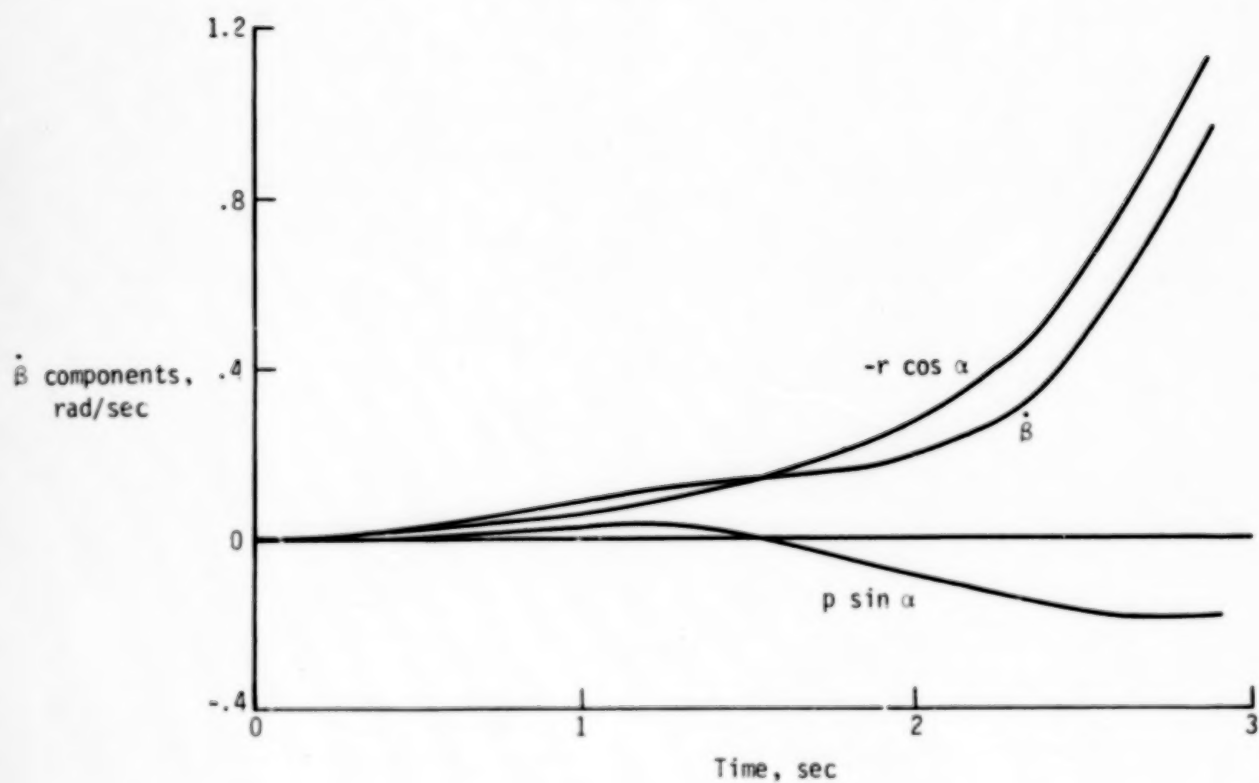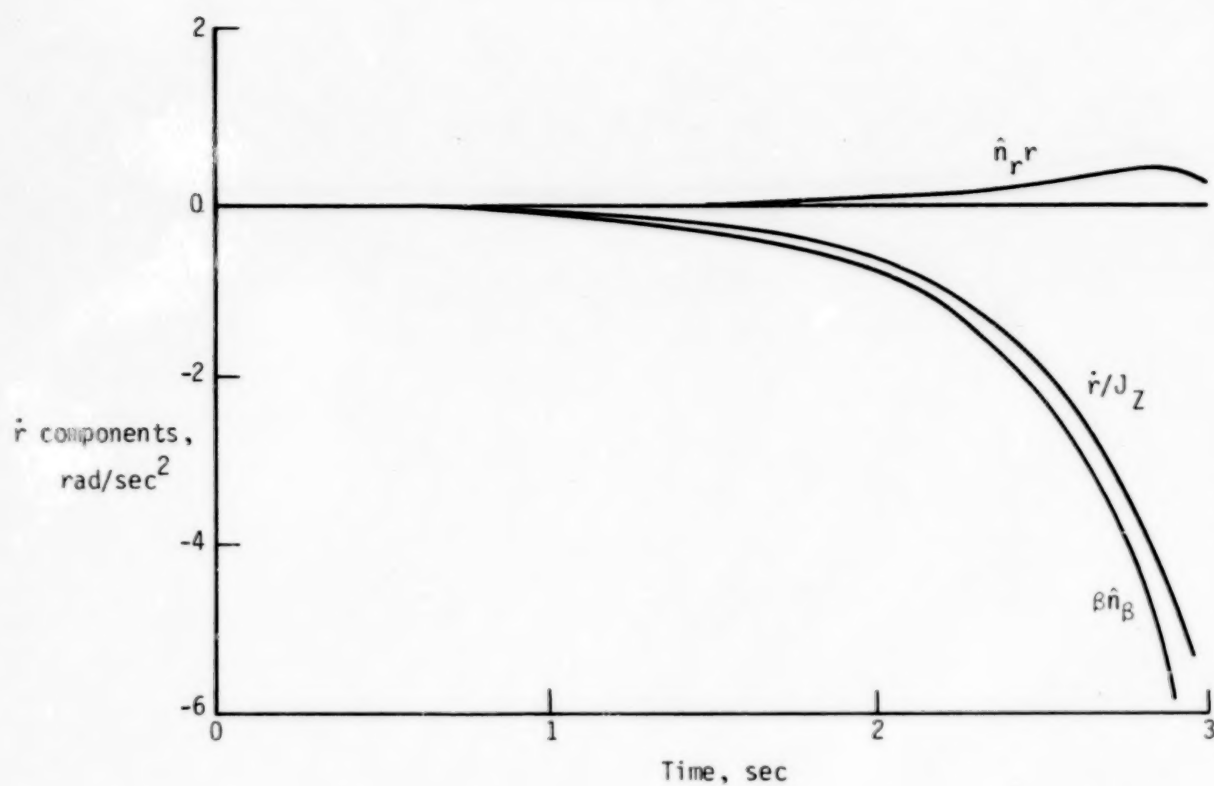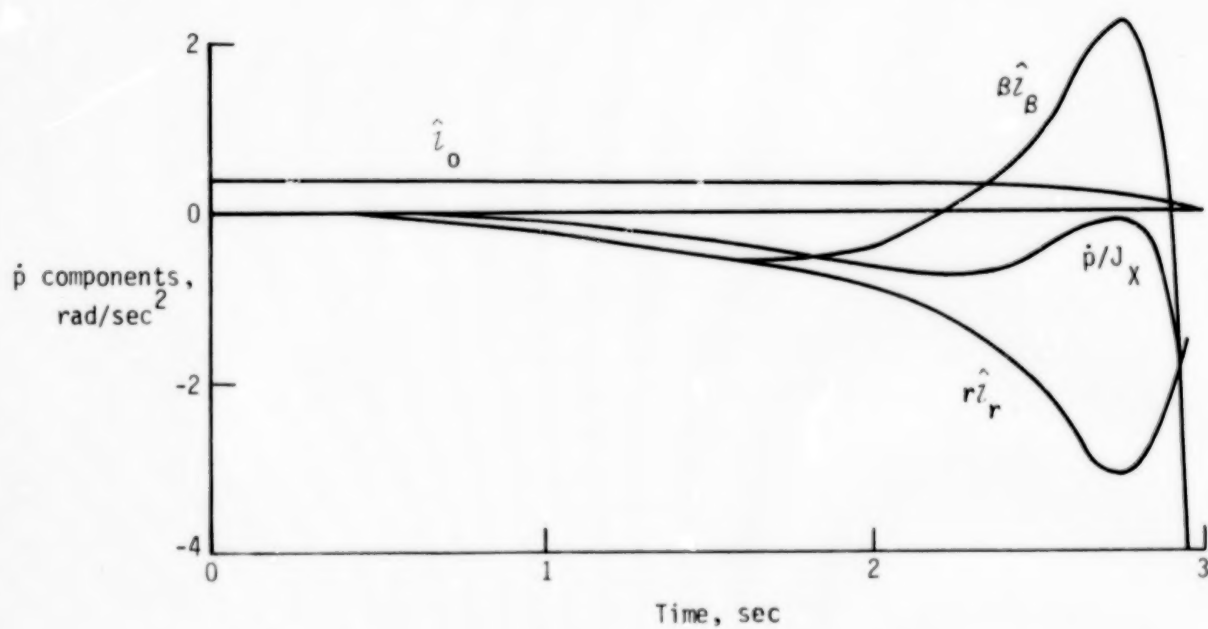Figure 6.- Concluded.
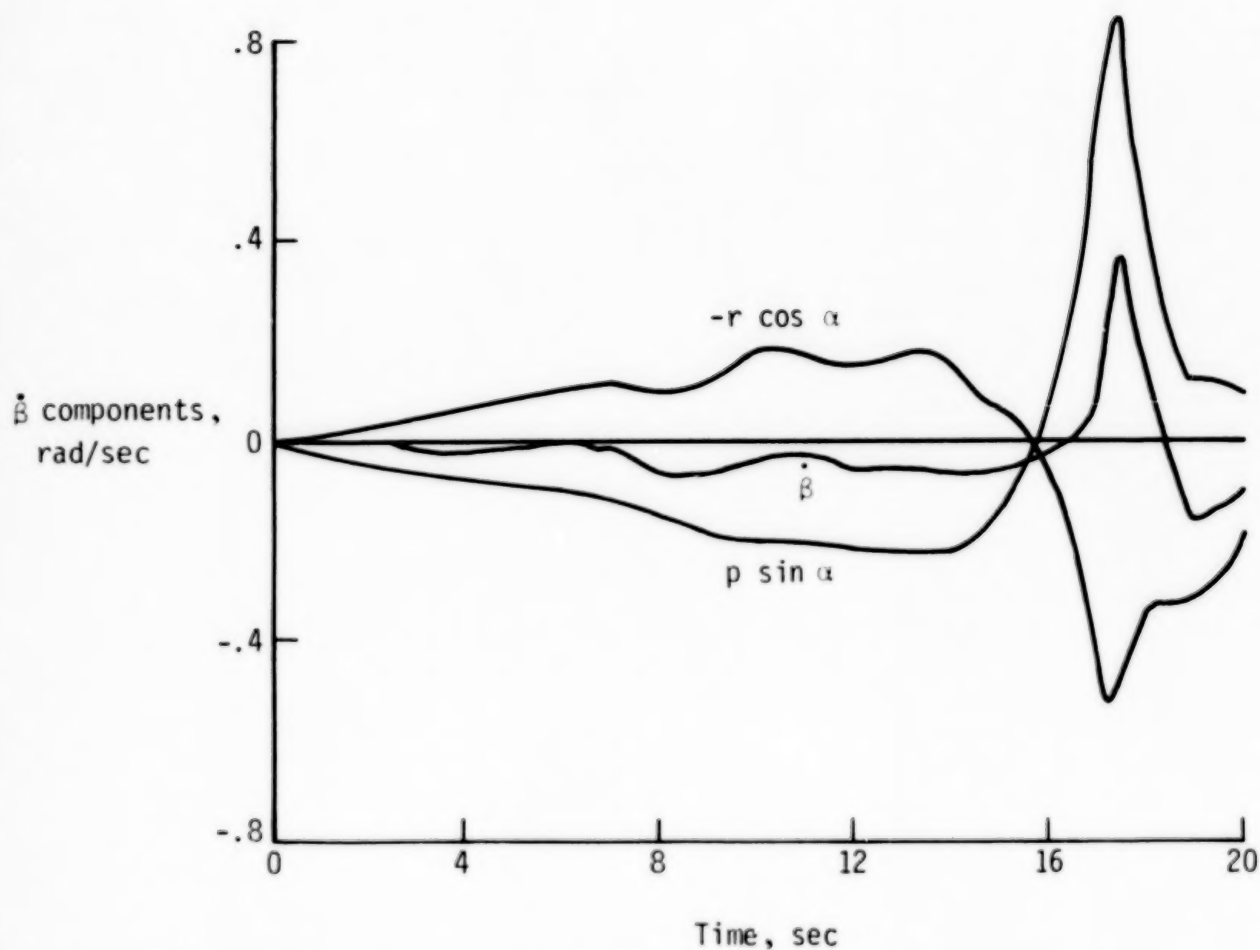
(a) Dominant components of $\dot{\beta}$.

Figure 7.- Dominant components of side-force, rolling-moment, and yawing-moment equations for response of figure 6.
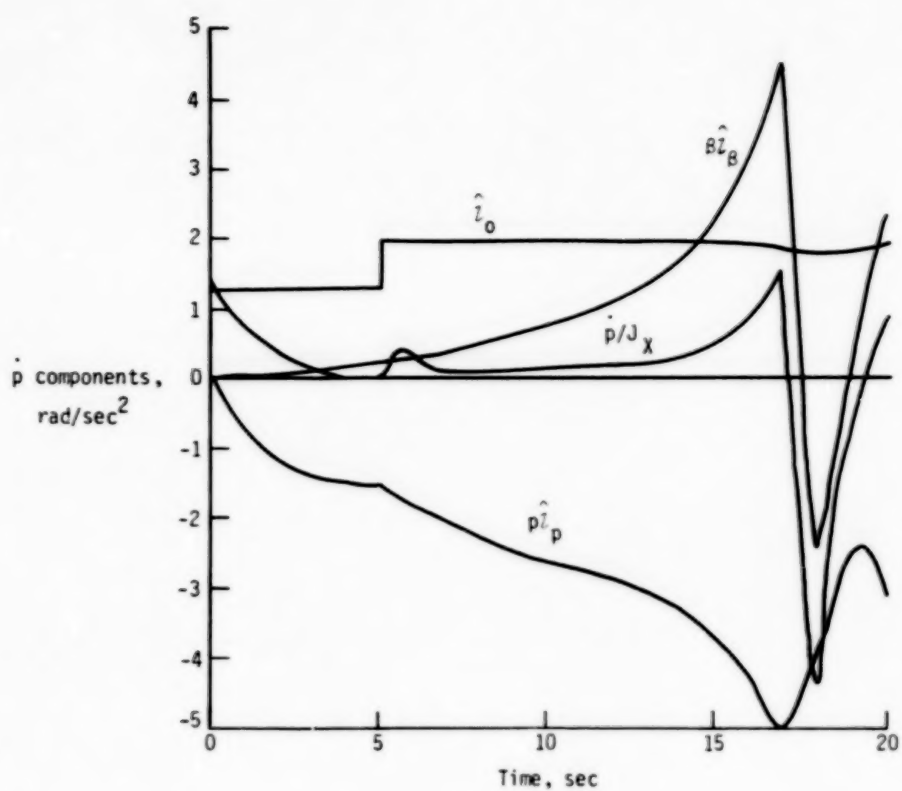
(b) Dominant components of $\dot{p}$.
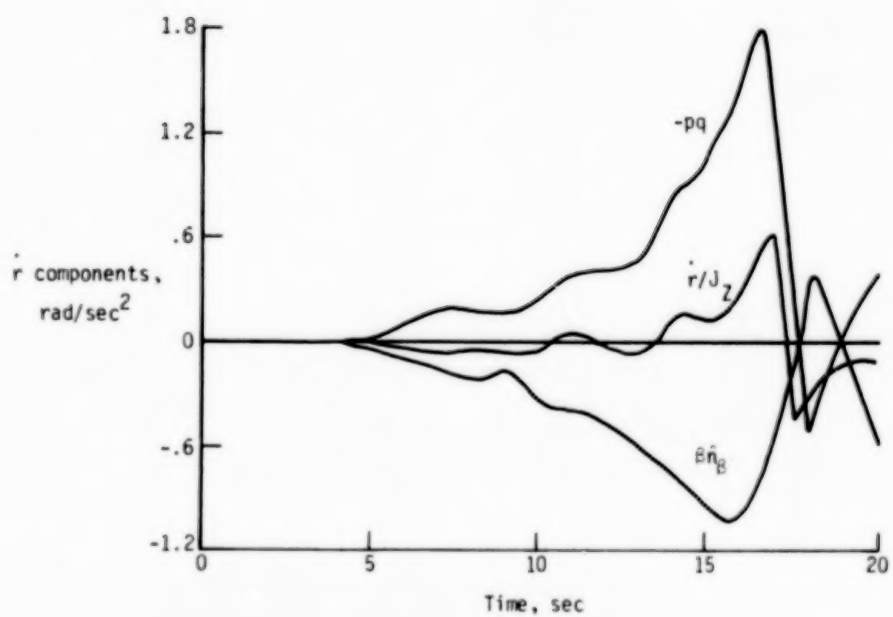


(c) Dominant components of $\dot{r}$.

Figure 7.- Concluded.
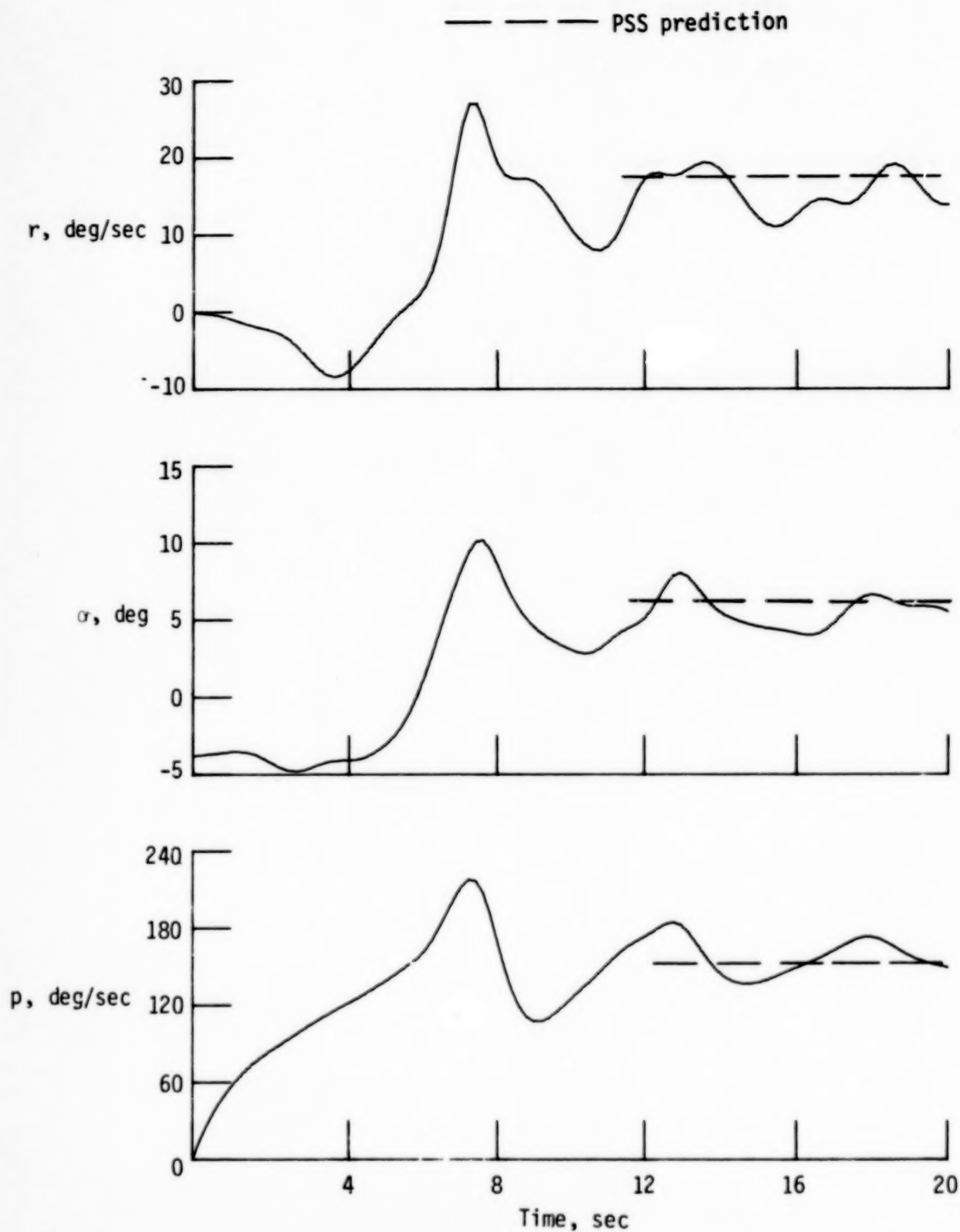
Figure 8.- Calculated responses initiated from pitch-down condition for $\delta_a = -15^o$. $\Delta\delta_e = 8^o$; $\alpha = -3.8^o$.
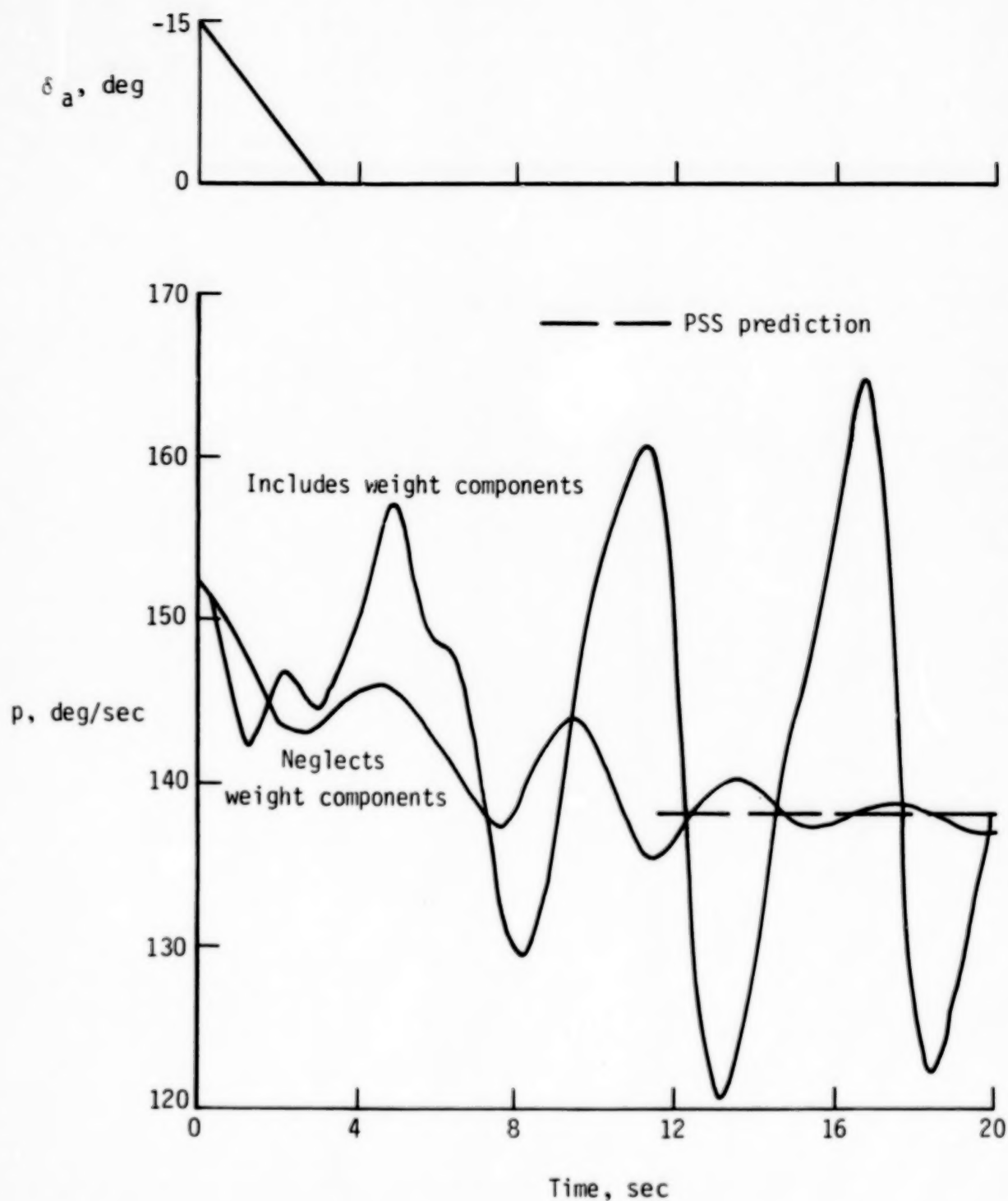
Figure 9.- Calculated roll-rate responses with and without varying weight components for $\Delta \delta_e = 8^o$. Initiated from $\Delta \delta_e = 8^o$ and $\delta_a = -15^o$ PSS condition.
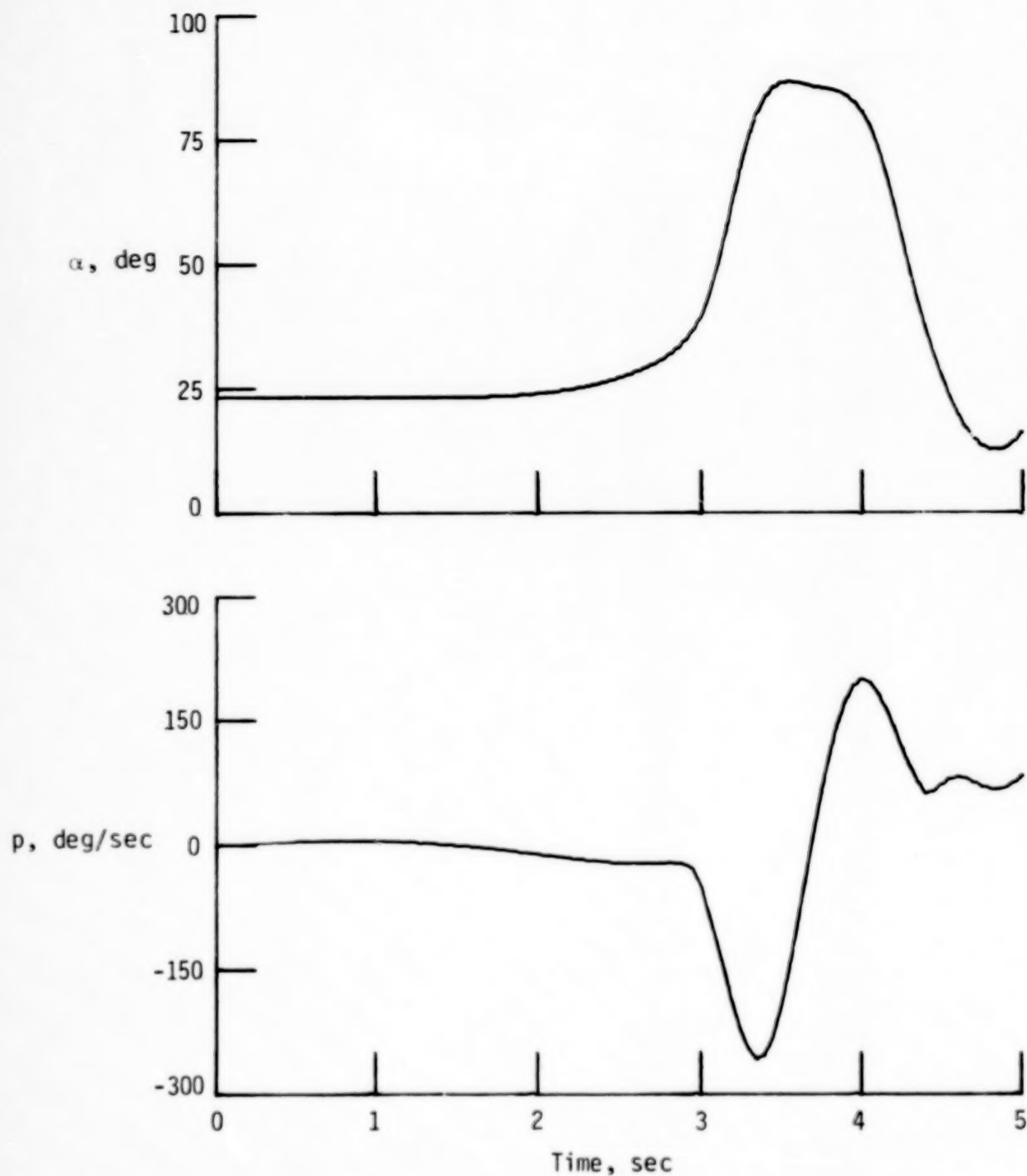
Figure 10.- Calculated responses initiated from pitch-up condition for $\delta_a = -5^o$. $\Delta\delta_e = -12^o$; $\alpha = 23.5^o$.
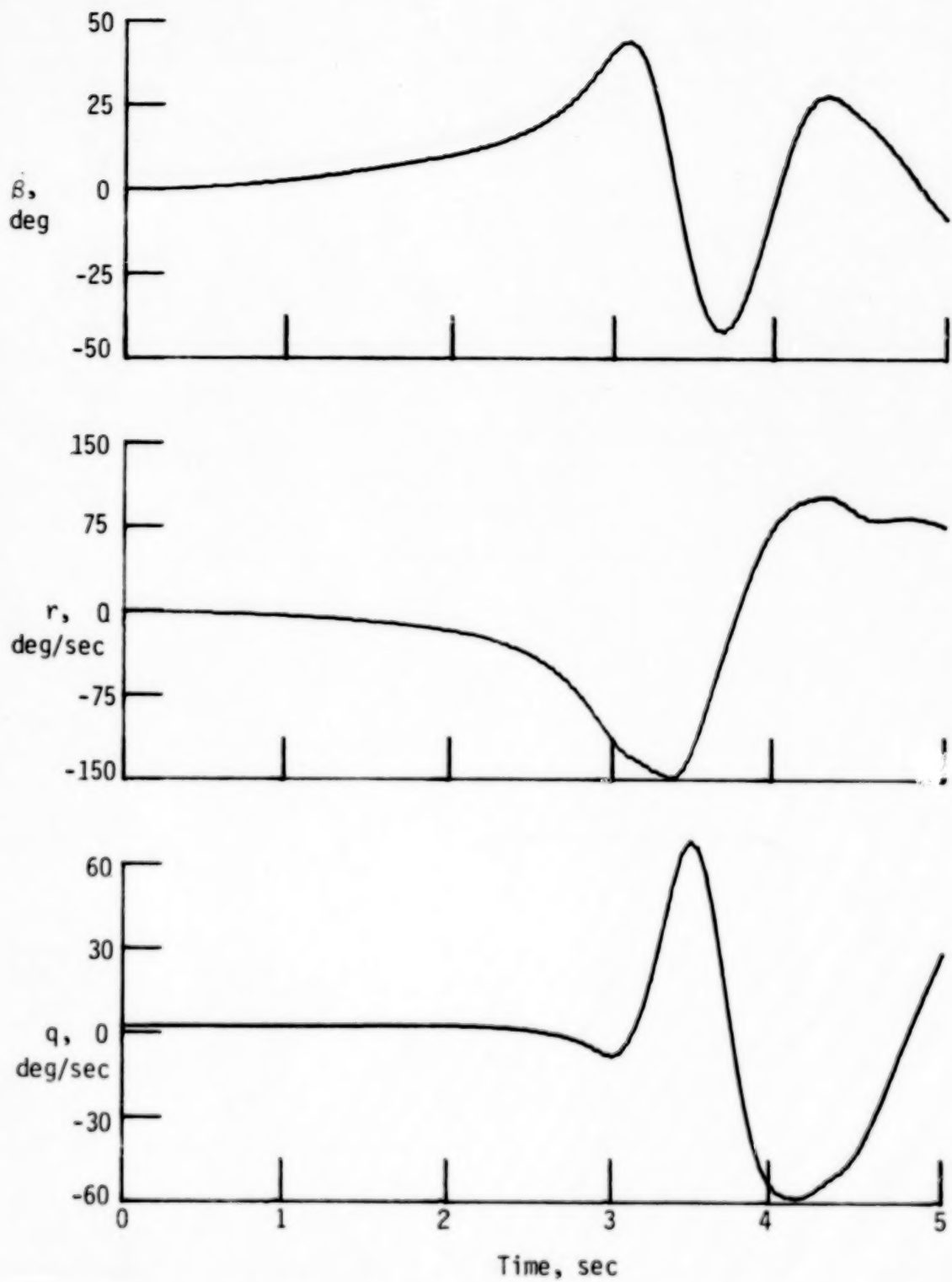
Figure 10.- Concluded.

(a) Dominant components of $\dot{\beta}$.

Figure 11.- Dominant components of side-force, rolling-moment, and yawing-moment equations for response of figure 10.
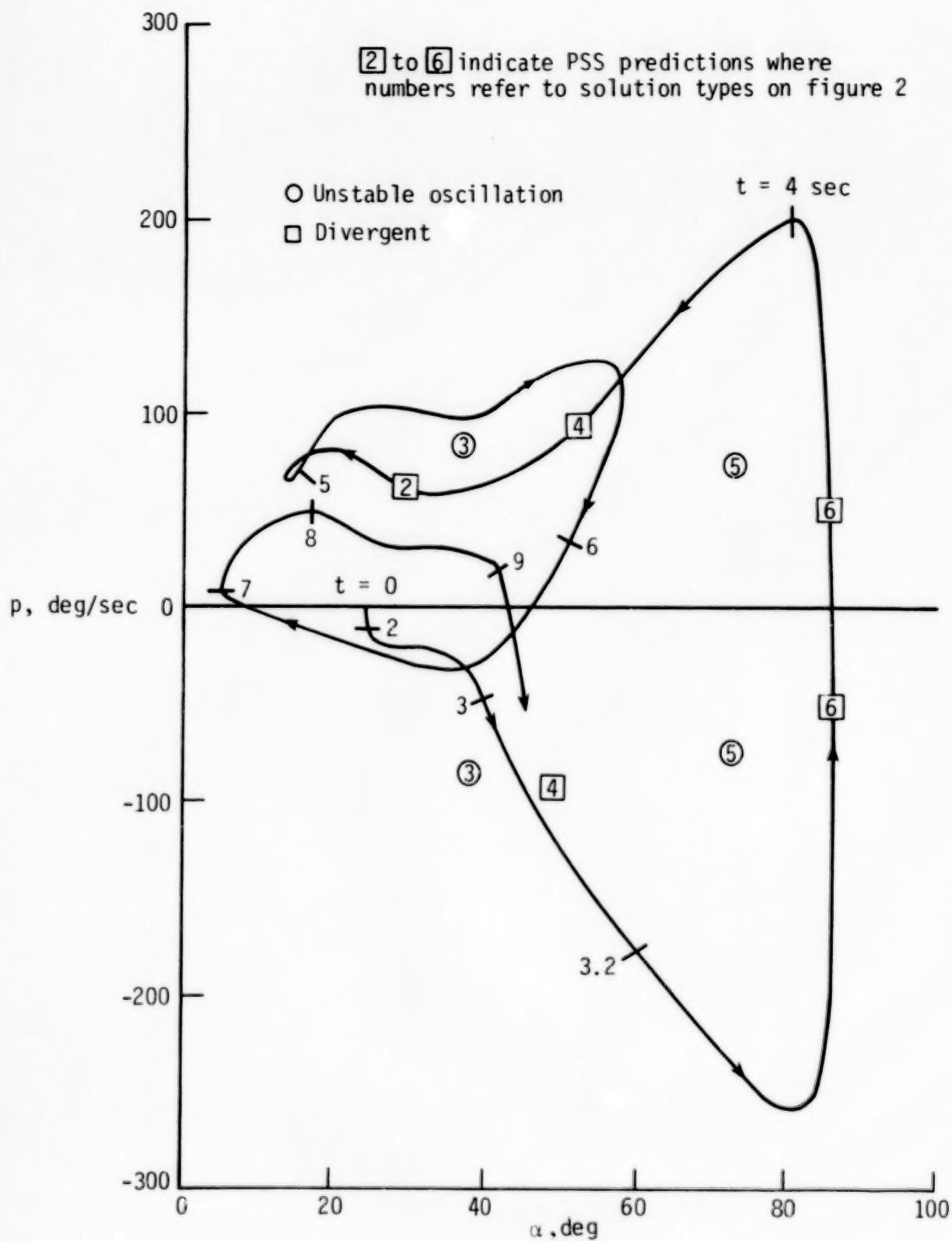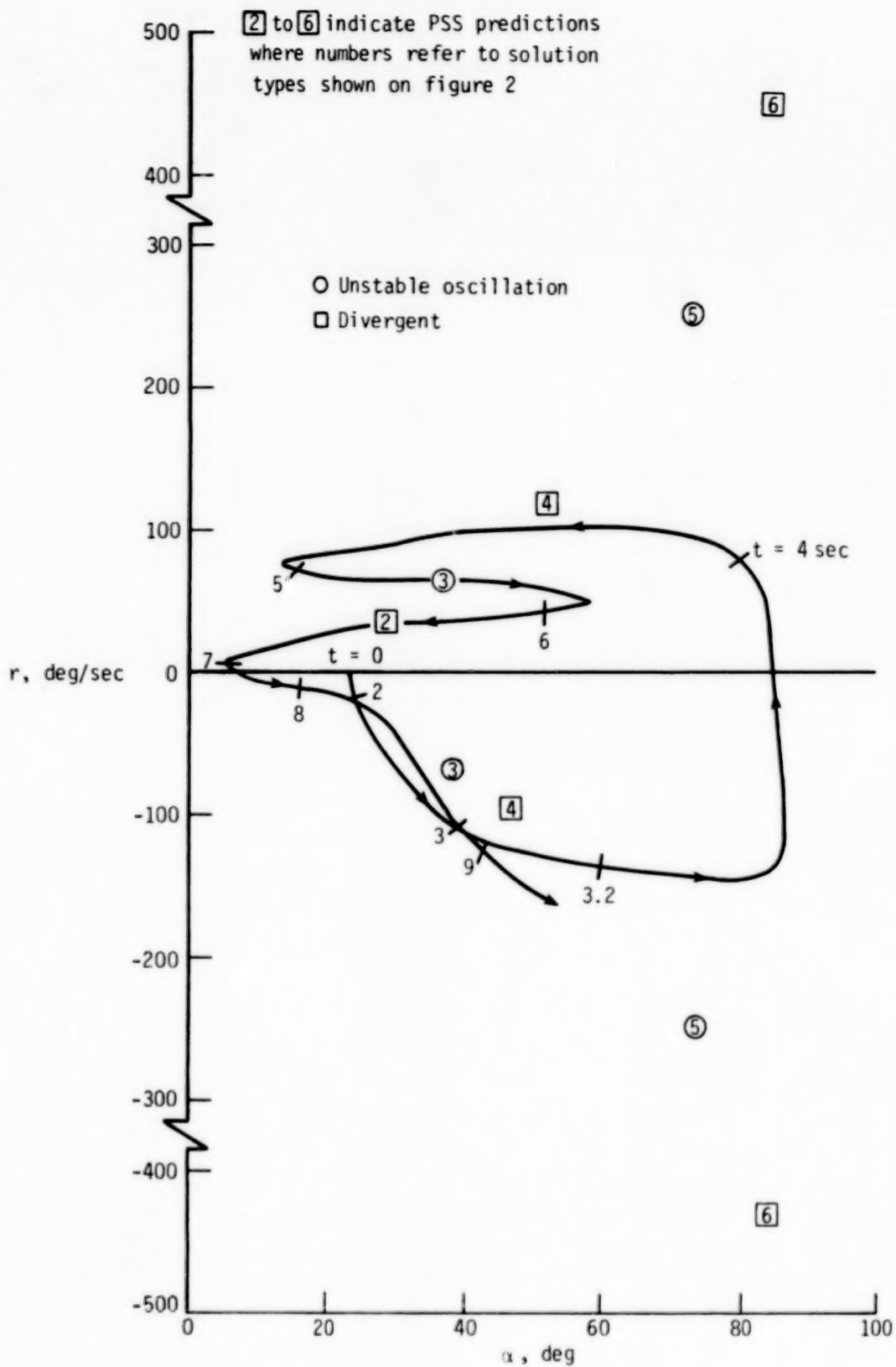
(b) Dominant components of $\dot{r}$.



(c) Dominant components of $\dot{p}$.

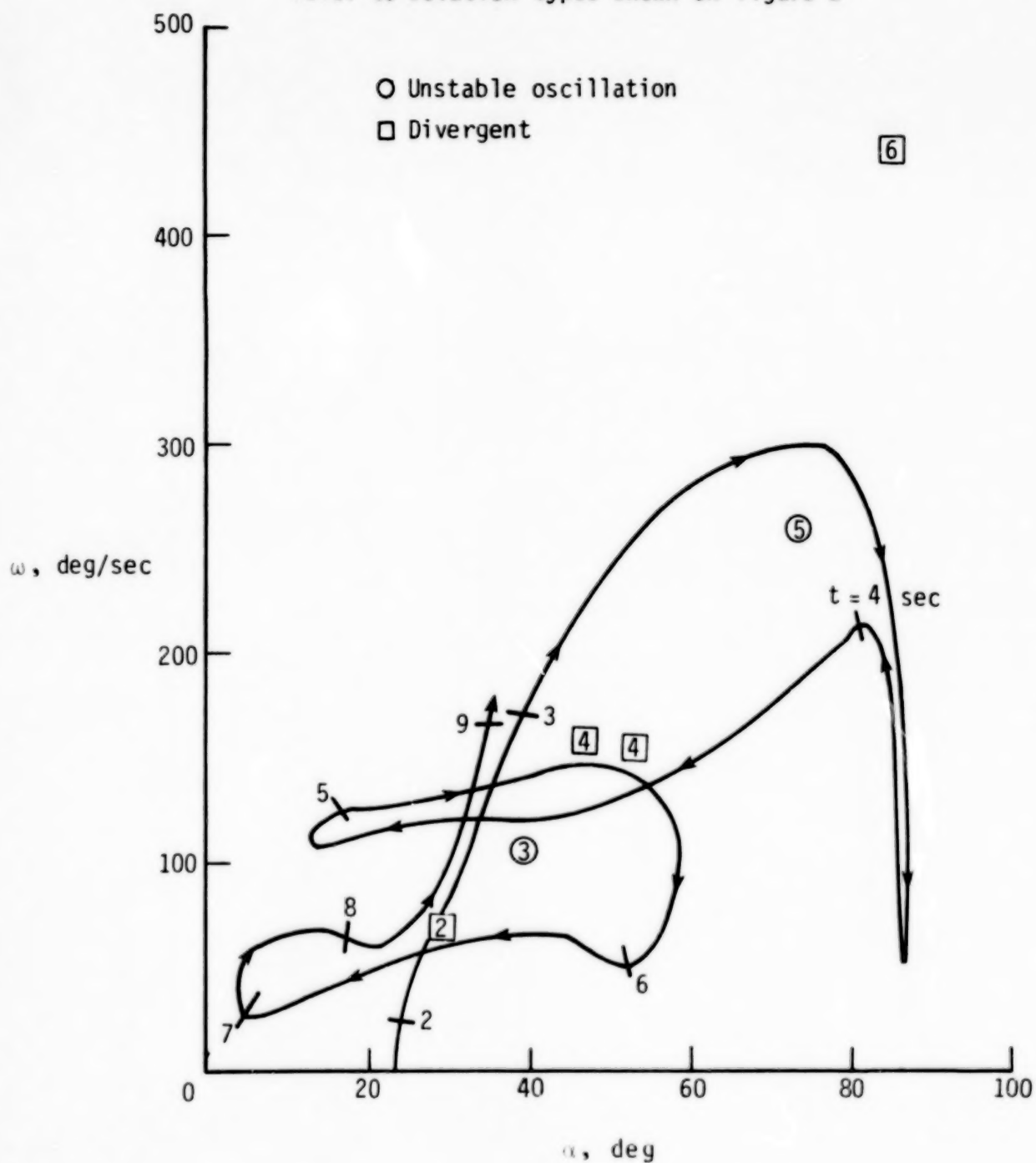Figure 11.- Concluded.

(a)  p  and  α  phase plot.

Figure 12.- Phase plots for pitch-up maneuver.  $\Delta\delta_e = -12°$;
$\delta_a = -5°$;  $\alpha = 23.5°$.

(b)  r  and  α  phase plot.

Figure 12.- Continued.

2 to 6 indicate PSS predictions where numbers
refer to solution types shown on figure 2

○ Unstable oscillation
□ Divergent

(c) $\omega$ and $\alpha$ phase plot.

Figure 12.- Concluded.

| 1. Report No. NASA TP-1758 | 2. Government Accession No. | 3. Recipient's Catalog No. |
|---|---|---|
| 4. Title and Subtitle PSEUDOSTEADY-STATE ANALYSIS OF NONLINEAR AIRCRAFT MANEUVERS | | 5. Report Date December 1980 |
| | | 6. Performing Organization Code 505-41-13-03 |
| 7. Author(s) John W. Young, Albert A. Schy, and Katherine G. Johnson | | 8. Performing Organization Report No. L-13743 |
| | | 10. Work Unit No. |
| 9. Performing Organization Name and Address NASA Langley Research Center Hampton, VA 23665 | | 11. Contract or Grant No. |
| | | 13. Type of Report and Period Covered Technical Paper |
| 12. Sponsoring Agency Name and Address National Aeronautics and Space Administration Washington, DC 20546 | | 14. Sponsoring Agency Code |

15. Supplementary Notes

16. Abstract

An analytical method has been developed for studying the combined effects of rotational coupling and nonlinear aerodynamics on aircraft response for specified control inputs. The method involves the simultaneous solution of two nonlinear equations which are functions of angle attack, roll rate, and control inputs. The method is applied to a number of maneuvers for a fighter-type aircraft. Time history responses verified the usefulness of the analysis for predicting a variety of response characteristics caused by interacting nonlinear aerodynamic and inertial effects, including spin conditions.

| 17. Key Words (Suggested by Author(s)) Nonlinear aircraft maneuvers Rotational coupling Nonlinear aerodynamics Spin conditions | 18. Distribution Statement Unclassified - Unlimited Subject Category 08 | | |
|---|---|---|---|
| 19. Security Classif. (of this report) Unclassified | 20. Security Classif. (of this page) Unclassified | 21. No. of Pages 61 | 22. Price A04 |

# END

February 18, 1981